Available online at www.sciencedirect.com

SciVerse ScienceDirect

Geochimica et Cosmochimica Acta 106 (2013) 344–363

Geochimica et Cosmochimica Acta

www.elsevier.com/locate/gca

The role of anaerobic respiration in the immobilization of uranium through biomineralization of phosphate minerals

Kathleen R. Salome [a], Stefan J. Green [b,e], Melanie J. Beazley [a,1], Samuel M. Webb [c], Joel E. Kostka [a,d], Martial Taillefert [a,*]

[a] School of Earth and Atmospheric Sciences, Georgia Institute of Technology, Atlanta, GA 30332-0230, United States
[b] DNA Services Facility, Research Resource Center, University of Illinois at Chicago, Chicago, IL, United States
[c] Stanford Synchrotron Radiation Lightsource, Menlo Park, CA 94025, United States
[d] School of Biology, Georgia Institute of Technology, Atlanta, GA 30332-0230, United States
[e] Department of Biological Sciences, University of Illinois at Chicago, Chicago, IL, United States

Received 18 July 2012; accepted in revised form 19 December 2012; available online 4 January 2013

Abstract

Although bioreduction of uranyl ions (U(VI)) and biomineralization of U(VI)–phosphate minerals are both able to immobilize uranium in contaminated sediments, the competition between these processes and the role of anaerobic respiration in the biomineralization of U(VI)–phosphate minerals has yet to be investigated. In this study, contaminated sediments incubated anaerobically in static microcosms at pH 5.5 and 7.0 were amended with the organophosphate glycerol-2-phosphate (G2P) as sole phosphorus and external carbon source and iron oxides, sulfate, or nitrate as terminal electron acceptors to determine the most favorable geochemical conditions to these two processes. While sulfate reduction was not observed even in the presence of G2P at both pHs, iron reduction was more significant at circumneutral pH irrespective of the addition of G2P. In turn, nitrate reduction was stimulated by G2P at both pH 5.5 and 7.0, suggesting nitrate-reducing bacteria provided the main source of inorganic phosphate in these sediments. U(VI) was rapidly removed from solution in all treatments but was not reduced as determined by X-ray absorption near edge structure (XANES) spectroscopy. Simultaneously, wet chemical extractions and extended X-ray absorption fine structure (EXAFS) spectroscopy of these sediments indicated the presence of U–P species in reactors amended with G2P at both pHs. The rapid removal of dissolved U(VI), the simultaneous production of inorganic phosphate, and the existence of U–P species in the solid phase indicate that uranium was precipitated as U(VI)–phosphate minerals in sediments amended with G2P. Thus, under reducing conditions and in the presence of G2P, bioreduction of U(VI) was outcompeted by the biomineralization of U(VI)–phosphate minerals and U(VI) sorption at both pHs.

1. INTRODUCTION

The United States Department of Energy (DOE) currently manages 120 nuclear legacy waste sites spread over 36 states contaminated with heavy metals and radionuclides, such as uranium (U) (DOE, 1997; NABIR, 2003). As the sheer volume of contaminated geomedia at these sites makes traditional remediation techniques (i.e. pump-and-treat, excavation) cost-prohibitive (Dawson and Gilman, 2001; Jardine et al., 2006; Mackay and Cherry, 1989), remedial efforts have focused on the development of alternative *in situ* technologies designed to immobilize contaminants in the subsurface.

As with other contaminants, the design of uranium *in situ* remediation techniques aims to capitalize on the

* Corresponding author.
E-mail address: mtaillef@eas.gatech.edu (M. Taillefert).
[1] Present address: Department of Biological Sciences, University of Alabama, Tuscaloosa, AL, United States.

0016-7037/$ - see front matter © 2013 Elsevier Ltd. All rights reserved.
http://dx.doi.org/10.1016/j.gca.2012.12.037

geochemical properties of uranium in natural waters to immobilize it in the subsurface. Uranium mobility in groundwater is largely driven by ligand complexation (i.e. carbonate), adsorption to metal oxides, and precipitation reactions (i.e. formation of phosphate minerals, reduced metal oxides). In oxic groundwater where U(VI) is the dominant oxidation state, uranium usually occurs as the highly mobile uranyl ion UO_2^{2+} (Langmuir, 1997). The dominant aqueous forms of uranyl in the environment include the free uranyl ion at low pH and positively charged hydroxyl complexes at circumneutral pH ($5 \leqslant pH \leqslant 6.5$) (Langmuir, 1997). At pH 5.0, aqueous U(VI) adsorbs strongly to manganese oxides given their low pH_{zpc} (Han et al., 2007) and even to ferric oxides despite the net positive charge of both uranyl hydroxide complexes and metal oxides (Hsi and Langmuir, 1985; Waite et al., 1994; Han et al., 2007). Ferric oxides represent one of the most important U(VI) sorbents in soils of the Oak Ridge Field Research Center (ORFRC), a well-studied nuclear legacy waste site in Oak Ridge, TN, and at pH 5.5 and 7.0 approximately 80% and 98% of U(VI) adsorbs to these soils (Barnett et al., 2002). In addition, the presence of inorganic phosphate may enhance U(VI) sorption to ferric oxides at low pH through the formation of ternary surface complexes (Payne et al., 1996; Cheng et al., 2004). In higher pH environments ($pH \geqslant 7.0$) and in the presence of elevated concentrations of carbonates, uranyl carbonate complexes represent the dominant form of U(VI) in solution (Langmuir, 1997). These complexes only minimally adsorb to iron oxides (Katsoyiannis, 2007), and the presence of elevated carbonate promotes both U(IV) and U(VI) mineral dissolution (De Pablo et al., 1999; Sowder et al., 2001; Liu et al., 2004; Ulrich et al., 2009). In addition, elevated calcium concentrations present in high pH environments may promote the formation of ternary calcium–uranyl–carbonate complexes, which further inhibit U(VI) sorption (Fox et al., 2006; Meleshyn et al., 2009; Stewart et al., 2010) and U(VI) reduction by lowering the reduction potential of uranium to less energetically favorable values (Brooks et al., 2003; Luo et al., 2007). Therefore, uranium mobility in circumneutral pH environments may be largely driven by carbonate dissolution and complexation reactions.

In reducing environments, uranium is either chemically or biologically reduced to insoluble U(IV) minerals, including uraninite (Langmuir, 1997; Finch and Murakami, 1999) or non-uraninite minerals (Bernier-Latmani et al., 2010; Fletcher et al., 2010; Sharp et al., 2011). At $pH > 6$, the surface-catalyzed chemical U(VI) reduction by Fe(II) adsorbed onto crystalline iron oxides (Liger et al., 1999; Behrends and Van Cappellen, 2005; Jeon et al., 2005; Regenspurg et al., 2009) and other minerals (Regenspurg et al., 2009; Chakraborty et al., 2010) may also occur. Dissolved sulfide (Mohagheghi et al., 1985; Ho and Miller, 1986; Kosztolanyi et al., 1996) and sulfide minerals (Wersin et al., 1994; Beyenal et al., 2004; Marsili et al., 2007) have also been shown to reduce U(VI) chemically. In addition, several strains of metal-reducing and sulfate-reducing bacteria are capable of reducing U(VI) (reviewed in Kostka and Green, (2011)), including members of the genus *Shewanella* (Lovley et al., 1991; Blakeney et al., 2000), *Desulfovibrio* sp. (Lovley and Phillips, 1992; Lovley, 1993), *Geobacter* sp. (Lovley et al., 1991; Jeon et al., 2004), and *Anaeromyxobacter dehalogens* (Sanford et al., 2007). Biologically-mediated reduction of U(VI), or bioreduction, is currently the primary *in situ* remediation technique studied for the immobilization of uranium in subsurface environments (Lovley et al., 1991; Lovley and Phillips, 1992; Ganesh et al., 1999; Fredrickson et al., 2000; Wade and DiChristina, 2000; North et al., 2004; Sanford et al., 2007), and *in situ* bioreduction of U(VI) has been demonstrated at the ORFRC (Wu et al., 2006b) and other contaminated sites (Senko et al., 2002). Unfortunately, bioreduction is inhibited at $pH < 7$ and in elevated nitrate concentrations (Finneran et al., 2002b; Wu et al., 2006a,b). In addition, the uraninite mineral product may not remain stable in fluctuating chemical conditions as uraninite is readily oxidized to the mobile U(VI) upon reintroduction of oxygen in groundwater recharge areas (Langmuir, 1997; Murphy and Shock, 1999) and by NO_2^- (Beller, 2005; Moon et al., 2007; Wu et al., 2010), $Fe(OH)_3$ (Senko et al., 2002; Wan et al., 2005; Senko et al., 2005b), and MnO_2 (Fredrickson et al., 2002) under reducing conditions. Thus, the long term instability of uraninite coupled with the inhibitory effects of co-contaminants on U(VI) reduction favors investigation of alternative remediation techniques applicable in both reducing and oxidizing conditions.

Biomineralization of insoluble U(VI)–phosphate minerals through the activities of microbial phosphatases represents a possible complementary bioremediation technique to bioreduction. U(VI) forms sparingly soluble and stable (Jerden and Sinha, 2003) phosphate minerals over a broad range of environmental conditions (pH 4–8) (Ohnuki et al., 2004; Zheng et al., 2006; Wellman et al., 2007), and uranium phosphate minerals have been identified in sediments from the ORFRC (Roh et al., 2000; Kelly et al., 2005; Stubbs et al., 2006) and the Hanford 300 Area facility, WA (Catalano et al., 2006; Arai et al., 2007), among others. As inorganic phosphate readily adsorbs to soils ($pH \leqslant \sim 7.0$) or precipitates as minerals ($pH \geqslant \sim 4.0$) ultimately decreasing the hydraulic conductivity of soils (Wellman et al., 2006), direct addition of inorganic phosphate to subsurface environments is not a viable field-scale remediation strategy. Thus, research has focused primarily on stimulating microbially-mediated phosphate production coupled to a chemical precipitation of sparingly soluble U(VI)–phosphate minerals (Beazley et al., 2007, 2009; Macaskie et al., 1995; Martinez et al., 2007; Montgomery et al., 1995; Shelobolina et al., 2009). To fulfill their phosphate requirements, most microorganisms produce phosphatase enzymes, a class of non-specific enzymes that catalyze the hydrolysis of organic phosphoester bonds in a broad range of chemical conditions (Rossolini et al., 1998). Uranium removal coupled to phosphatase activity has been demonstrated in both aerobic and anaerobic conditions and at both acidic and circumneutral pH by the facultative anaerobe *Rahnella* sp. Y9602 (Beazley et al., 2007, 2009; Martinez et al., 2007) and in low-pH aerobic conditions by *Citrobacter* sp. (Macaskie et al., 1995; Montgomery et al., 1995). In addition, uranium removal in aerobically-maintained contaminated sediments has been achieved through

stimulation of the phosphatase activities of indigenous bacteria (Shelobolina et al., 2009; Beazley et al., 2011). As phosphatases may also be activated in anaerobic conditions (Rossolini et al., 1998), U(VI)–phosphate biomineralization may compete with bioreduction in the presence of G2P. Interestingly, the competitive interaction between these two processes has yet to be investigated.

In this study, a combination of X-ray absorption spectroscopy, solid-phase extractions, and bulk chemical analyses was used to determine whether nitrate-, iron-, or sulfate-reducing conditions are most conducive to uranium removal through the activity of endogenous microbial phosphatases in contaminated sediments from the ORFRC. In addition, the competition between uranium reduction and the biomineralization of U(VI)-phosphate minerals under varying electron accepting conditions in both low and circumneutral pH environments was examined.

2. EXPERIMENTAL

2.1. Materials and site description

Contaminated sediments were collected during installation of a monitoring well in Area 3 of the ORFRC (well number: FWB120-08-40, core depth: 21–23′; courtesy of D. Watson, ORNL). Soil mineralogy of neighboring wells indicates a bulk soil particle size distribution (~1.5 m depth) as 31% sand, 50% silt, and 19% clay (Barnett et al., 2000). In addition, bulk soil Mn and Fe content in Oak Ridge sediments have been quantified as 0.36 g/kg and 25.8 g/kg, respectively (Barnett et al., 2000), and uranium-bearing Fe and Mn minerals in Area 3 Oak ridge soils have been identified as polycrystalline ferrihydrite and goethite and poorly crystalline mixed Mn–Fe oxides (Stubbs et al., 2006). As Area 3 sediments are located closest to the former waste disposal ponds, they are generally characterized by low pH and high nitrate levels (Brooks, 2001). Chemical information for well FWB120 remains unavailable; however, the nearest neighboring well (~1 m) displays an average pH of 3.4, nitrate concentration of 30.4 mM, and sulfate concentration of 19.7 mM. Sediment cores were stored in the dark at 4 °C and remained sealed until incubation.

2.2. Experimental design

To simulate a variety of environmental conditions, static microcosms containing 125 g of contaminated ORFRC sediments homogenized under controlled atmosphere (1% H_2, 5% CO_2, 94% N_2) were incubated in duplicate in 1-L borosilicate glass reactors containing sterile artificial groundwater for a period of 70 days. In each treatment, 500 mL of artificial groundwater containing 17.1 mM NaCl, 2.0 mM $MgCl_2{\cdot}6H_2O$, 680 μM $CaCl_2{\cdot}2H_2O$, and 6.7 mM KCl was first degassed using UHP N_2, sealed, and autoclaved. After cooling, filter-sterilized aliquots of selenite–tungstate solution (0.1%), trace elements solution (0.1%, Table S1, (Bak, 1992)), $NaHCO_3$ (5 mM), and either 2-(*N*-Morpholino)ethanesulfonic acid (MES, 50 mM, pH 5.5) or 4-(2-hydroxyethyl)-1-piperazineethanesulfonic acid (HEPES, 50 mM, pH 7.0) were added to autoclaved groundwater in the presence or absence of filter-sterilized solutions of glycerol-2-phosphate (G2P) (Sigma Aldrich) and uranyl acetate (Spectrum) (Table 1). Reactors were buffered at pH 5.5 or 7.0 to establish conditions favorable to both U(VI)–phosphate biomineralization (pH 5.5) and bioreduction (pH 7.0). Excluding G2P, no external electron donor was added to the system. Reactors were sealed from the controlled atmosphere within an hour after addition of the reactants, such that the incubations were not significantly affected by H_2 and CO_2 gases. Sealed duplicate reactors were homogenized to ensure uniform groundwater composition prior to static incubation at room temperature in the dark.

Table 1
pH, U(VI), G2P, and external terminal electron acceptor (TEA) conditions in each incubation conducted in duplicate in artificial groundwater.

Treatment	pH	[U(VI)]	[G2P]	[TEA]
U-amended control	5.5/7.0	300 μM	0 mM	0 mM
G2P-amended reactor	5.5/7.0	300 μM	5.0 mM	0 mM
NO_3^--amended reactor	5.5	300 μM	5.0 mM	7.0 mM NO_3^-
NO_3^--amended reactor	7.0	300 μM	0 mM	7.0 mM NO_3^-
SO_4^{2-}-amended reactor	5.5/7.0	300 μM	5.0 mM	9.4 mM SO_4^{2-}

At each time point, the following sampling protocol was followed to ensure that all samples were maintained anaerobic at all times. Microcosm sediment and groundwater were homogenized, and a subsample of the microcosm mixture was extracted under anaerobic atmosphere (1% H_2, 5% CO_2, and 94% N_2) through a septum using a polypropylene syringe with Teflon plunger (HSW) and a 18 gauge stainless steel needle (B & H). An aliquot of the homogenized mixture was added to a 0.5 M HCl solution to extract total Fe(II). The remaining mixture was centrifuged at 3300 rpm for 5 min. The supernatant was filtered through a 0.2 μm pore size polyethersulfane membrane filter (Puradisc, Whatman) and reserved for pH measurement (data not shown) and analysis of phosphate and nitrite. Other filtered aliquots were diluted in 2% trace metal grade nitric acid for uranium analysis or preserved in 0.1 M HCl and stored at 4 °C until dissolved Fe(II) quantification. The remaining filtered supernatant was frozen until analysis of sulfate, nitrate, and G2P. Finally, following completion of the incubations, sediments were collected for solid-phase chemical extraction, X-ray absorption near-edge spectroscopy (XANES), and extended X-ray absorption fine structure (EXAFS) analysis. Sediments were preserved at −80 °C and under UHP N_2 atmosphere in Mason jars until analysis.

2.3. Analytical methods

2.3.1. Aqueous phase chemical composition

Dissolved uranium was measured in duplicate using an Agilent 7500a Series inductively coupled plasma mass

spectrometer (ICP-MS). Standards were prepared using uranyl acetate (Spectrum) acidified in 2% trace metal grade nitric acid (Fisher). Holmium and bismuth were used as internal references in both standards and samples (SPEX certiPrep), and 2% trace metal grade nitric acid blanks and calibration check standards were used as quality controls. Phosphate, nitrite, and total/dissolved Fe(II) were quantified colorimetrically with a Milton Roy Spectronic 501 spectrophotometer. Phosphate was measured using the molybdenum blue method (Murphy and Riley, 1962), nitrite was measured using a sulphanilamide/NED reagent mixture immediately after sampling (Grasshoff, 1983), and Fe(II) was measured using the ferrozine method (Stookey, 1970). Adsorbed Fe(II) was quantified by difference of total Fe(II), measured in unfiltered acidified samples, and dissolved Fe(II) determined in filtered samples. Sulfate, nitrate, and G2P were measured by ion chromatography using a Dionex GP-50 HPLC pump and conductivity detector (Dionex, CD-20) coupled to an Analytical Instrument Systems, Inc. integrator (LCC 100). An anion exchange analytical column (Dionex AS14, 4 × 250 mm) and guard column (Dionex AG14, 4 × 50 mm) were used in line with an AMMS-300 (4-mm, Dionex) suppressor. Operating conditions included a 10% acetonitrile, 1 mM $NaHCO_3$, and 3 mM Na_2CO_3 buffer eluent with a 1 mL min^{-1} flow rate and a 25 mN H_2SO_4 regenerant. All standard deviations reported for dissolved species represent the range of average concentrations found in duplicate reactors.

2.3.2. Rate constant calculations and thermodynamic modeling

Rate constants, k_{obs}, for NO_3^- consumption, G2P consumption, and U removal were calculated assuming pseudo-first-order reactions using the linear regression of the natural log of concentrations as a function of time (see details in Supplementary information). The error reported for rate constants was propagated to include variations between duplicate incubations and standard error of the unweighted slope of linear regressions. Due to the apparent two-phased uranium removal, two separate uranium rate constants were calculated for pH 5.5 reactors; U_0 represents the rate constant calculated for days 0–4 and U_7 represents the rate constant calculated for days 7–31. Thermodynamic equilibrium calculations were performed in MINEQL+ (Schecher and McAvoy, 2001) for each reactor treatment. The theoretical composition of artificial groundwater, modified to reflect the different treatments (Table 1), was included as the background solution in the thermodynamic calculations. For these calculations, total ΣPO_4^{3-} concentrations in all G2P-containing reactors were estimated assuming complete hydrolysis of the organophosphate compound, and total Fe(II) detected at 7 days was used to estimate the maximum Fe(II) production. Adsorption onto amorphous iron oxides was included using a double-layer sorption model with both low affinity and strong affinity sites and solid concentrations that reflected the composition of ORFRC soils (Barnett et al., 2002). Ionic strength was calculated, and the system was assumed to be closed to the atmosphere with a pH of 5.5 or 7.0 and total dissolved inorganic carbon concentrations fixed at 5 mM.

2.3.3. Solid phase uranium characterization

Solid phase uranium and phosphate eventually associated with the solid phase were quantified in duplicates in sediments collected following 70 days of incubation using a modified sequential extraction technique of Tessier et al. (1979). The following procedure was performed sequentially: (1) 4 mL of 1.0 M $MgCl_2$ (pH 7.0) was added to ~0.5 g sediment and agitated at 20 °C for 1 h to extract loosely adsorbed uranium; (2) 4 mL of 1.0 M sodium acetate (adjusted to pH 5.0 with 1.0 M HCl) was added and agitated at 20 °C for 5 h to dissolve uranium–phosphate minerals (Beazley et al., 2011); (3) 10 mL of 0.04 M $NH_2OH{\cdot}HCl$ in 25% (v/v) acetic acid was added and agitated at 96 °C for 6 h to remove Fe- and Mn-associated uranium; (4) 1.5 mL of 0.02 M HNO_3 and 2.5 mL of 30% H_2O_2 (pH 2.0) were added and agitated at 96 °C for 2 h, a second 1.5 mL aliquot of 30% H_2O_2 (pH 2.0) was added and agitated at 96 °C for 3 h, and a third 5 mL aliquot of 2.5 M NH_4OAc in 20% (v/v) HNO_3 was added and agitated at 20 °C for 1 h to extract uranium bound to organics; and (5) 5 mL of 15.8 M HNO_3 was added and maintained at 85 °C for 3 h to extract the residual fractions (Gleyzes et al., 2002). After each extraction step, samples were centrifuged (1380*g* for 10 min), and supernatants were filtered (0.2 μm, PES Puradisc Whatman) and reserved for uranium analysis by ICP-MS and for phosphate quantification using the spectrophotometric technique of Murphy and Riley (1962). The pH of the samples for phosphate quantification in each extract was adjusted to ~4.0 with NaOH (10.0 M) or HCl (12.0 M) to allow for color development. Standards were prepared in extraction media and treated as described above.

X-ray absorption spectroscopy (XAS) was performed at the Stanford Synchrotron Radiation Lightsource (SSRL). Final samples (70 days) from the U-amended controls, the G2P-amended reactors, nitrate-amended reactors, and the sulfate-amended reactors at both pH 5.5 and 7.0 were characterized by XAS, and an initial sample ($T = 0$ days) from pH 5.5 G2P-amended reactors was also examined. Sediment samples were loaded into windowed Lexan sample holders, sealed with Kapton tape in an anaerobic chamber (Coy Laboratory Instruments, Inc.), and maintained anoxic in a sealed jar for transport to SSRL and under N_2 atmosphere at the beam line. Uranium L_{III}-edge XAS spectra were collected at SSRL beam line 10–2 using a focused X-ray beam with a 23 keV harmonic rejection cutoff and a 13 element Ge detector. The incident energy was selected with a Si(220) monochromator crystal. Transmission and fluorescence data were collected simultaneously. Detection limits of around 5% weight are achieved in these conditions at beam line 10–2. All EXAFS data were reduced using SIXPACK (Webb, 2005). Phase and amplitude files for EXAFS fittings were created with FEFF7 (Zabinsky et al., 1995; Ankudinov et al., 1998). Theoretical models were based on scattering paths expected for autunite-type group minerals (Catalano and Brown, 2004) and U(VI) adsorbed to iron oxihydroxides (Waite et al., 1994). The models were first tested on known chernikovite and U–$Fe_{(ads)}$ samples to ensure good agreement with previous fittings (Beazley et al., 2009, 2011). The U = Oax = U = Oax transoxido multiple

scattering path (Allen et al., 1996; Hudson et al., 1996; Bargar et al., 2000) was included in all fits. The axial oxygen coordination number (N) for all reactors was set at two (Beazley et al., 2007, 2009, 2011; Webb et al., 2006). To aid comparison between samples, the Debye–Waller factors (σ) were fixed for shells other than axial oxygen, a common practice for uranium EXAFS (Bargar et al., 2000; Webb et al., 2006; Beazley et al., 2009, 2011). The addition of shells was considered to improve the quality of the EXAFS fit if a reduction in the reduced chi-square was observed (Webb et al., 2005, 2006). As Mn and Fe display similar backscattering intensities and phases in EXAFS, it is unlikely to distinguish these two elements during the fitting procedure. Thus, rather than distinct Fe and Mn shells, a "sum" of Fe/Mn like neighbors was reported for all the treatments.

3. RESULTS

3.1. Aqueous species

The pH remained constant for the duration of the experiments in both pH 5.5 and 7.0 reactors (data not shown). In all treatments without addition of external terminal electron acceptors (TEAs), background nitrate and sulfate concentrations exchanged from the original sediment after 3 h of equilibration averaged 450 μM and 800 μM, irrespective of the pH of the incubations (Fig. 1A–D). Although sulfate and nitrate were present in the U-amended controls, both nitrate and sulfate reduction were negligible without G2P addition (Fig. 1A–D), even in pH 7.0 incubations in the presence of 7 mM NO_3^- (Fig. 1D). After a phase lag of 15 days, the presence of G2P stimulated nitrate reduction at both pH 5.5 and 7.0 (Fig. 1E–H) but not sulfate reduction, even in treatments containing elevated sulfate concentrations (Fig. 1A and B), and complete depletion of nitrate was observed in G2P-containing reactors without NO_3^- addition after 39 days of incubation (Fig. 1C and D). Pseudo-first-order rate constants for nitrate reduction in G2P-containing reactors unamended with nitrate were calculated to be 0.04 ± 0.01 d^{-1} and 0.07 ± 0.03 d^{-1} at pH 5.5 and 7.0 (Table 2). Although nitrate was removed in the sulfate-amended reactors, only ephemeral accumulation of nitrite was observed, while traces of nitrite were observed in the G2P-amended reactors with no external TEA (Fig. 1C and D). In the nitrate-amended reactors at pH 5.5, nitrate concentrations were reduced from 7 to 2 mM over 70 days (Fig. 1C) with a pseudo-first-order rate constant of 0.02 ± 0.004 d^{-1} (Table 2), and the accumulation of 4 mM nitrite was observed after a small phase lag (Fig. 1C).

Aqueous Fe(II) remained constant at ~10 μM in both pH 5.5 and pH 7.0 reactors throughout the 21 day sampling period (Fig. 1E and F). In all pH 5.5 reactors, adsorbed Fe(II) remained constant at 15 μM until day 7 when a steep increase to 100 μM was observed (Fig. 1E). A much more pronounced increase in adsorbed Fe(II) was detected in all pH 7.0 reactors, irrespective of the TEA present, with concentrations as high as 1.1 mM (Fig. 1F). A pseudo-first-order rate constant for Fe(III) reduction of 0.61 ± 0.05 d^{-1} was calculated from total Fe(II) produced at pH 5.5, while an average pseudo-first-order rate constant of 1.34 ± 0.04 d^{-1} was estimated for all treatments at pH 7.0 (Table 2). The increase in adsorbed Fe(II) was followed by a steady decrease to ~65 μM after 21 days of incubation in all reactors at both pH (Fig. 1E and F). The same trends were observed in all reactors, regardless of the presence or absence of G2P.

Although G2P-containing reactors were amended with 5 mM G2P, initial aqueous G2P concentrations averaged only 1 mM at pH 5.5 and 2.3 mM at pH 7.0 (Fig. 1G and H), indicating adsorption of G2P onto ORFRC sediments is more significant at low pH. Complete removal of dissolved G2P was observed after 39 days of incubation (Fig. 1G and H), and the pseudo-first-order rate constant for G2P consumption at pH 5.5 and 7.0 averaged 0.05 ± 0.02 d^{-1} and 0.10 ± 0.02 d^{-1}, respectively (Table 2). Dissolved phosphate was not detected in the U-amended controls or the pH 7.0 nitrate-amended reactors without G2P (Fig. 1H). However, in all G2P-containing reactors at pH 5.5, up to 120 μM inorganic phosphate accumulated after 30 days of incubation followed by a slow linear decrease to 50 μM by day 70 (Fig. 1G). Alternatively, in all pH 7.0 G2P-containing reactors, inorganic phosphate accumulated up to 350 μM after 39 days of incubation and remained around the same concentration for the remainder of the experiments (Fig. 1H). This observed accumulation of phosphate is ~90% lower than expected if mass balance with G2P consumption was conserved, indicating that at both pH a significant fraction of phosphate was removed by adsorption onto the solid phase, uptake by microbial populations, and/or precipitation of phosphate minerals.

All reactors amended with 300 μM U but not G2P at both pH initially contained only 2 μM uranium in solution, and uranium concentrations remained at 2 μM for the duration of the incubations (Fig. 2A). As U(VI) was instantaneously removed by precipitation or adsorption onto the solid phase and no temporal change in uranium concentration was observed in these treatments, the pseudo-first-order rate constants for this removal process were reported as zero (Table 2). In the presence of G2P, however, pH 5.5 reactors amended with 300 μM uranium displayed approximately 55 μM uranium in solution at time zero, while the same reactors at pH 7.0 displayed only 15 μM (Fig. 2A). Rapid uranium removal to <0.2 μM was observed in G2P-containing reactors at pH 5.5, and U remained immobilized for the duration of the experiment regardless of the type and presence of terminal electron acceptor (TEA) (Fig. 2A). Interestingly, uranium removal at pH 5.5 was divided into two distinct phases, an initial phase between 0 and 4 days during which U(VI) removal occurred with an average pseudo-first-order rate constant of 0.41 ± 0.12 d^{-1} for all treatments, and a second phase between 7 and 30 days during which removal occurred with an average pseudo-first-order rate constant 0.10 ± 0.02 d^{-1} for all treatments (Table 2 and Fig. 2B). In contrast, the initial 15 μM uranium present in pH 7.0 reactors was steadily titrated out of solution over the 70 day sampling period to <0.2 μM (Fig. 2A) with a pseudo-first-order rate constant of 0.06 ± 0.01 d^{-1} (Table 2) regardless of the presence or absence of elevated sulfate concentrations.

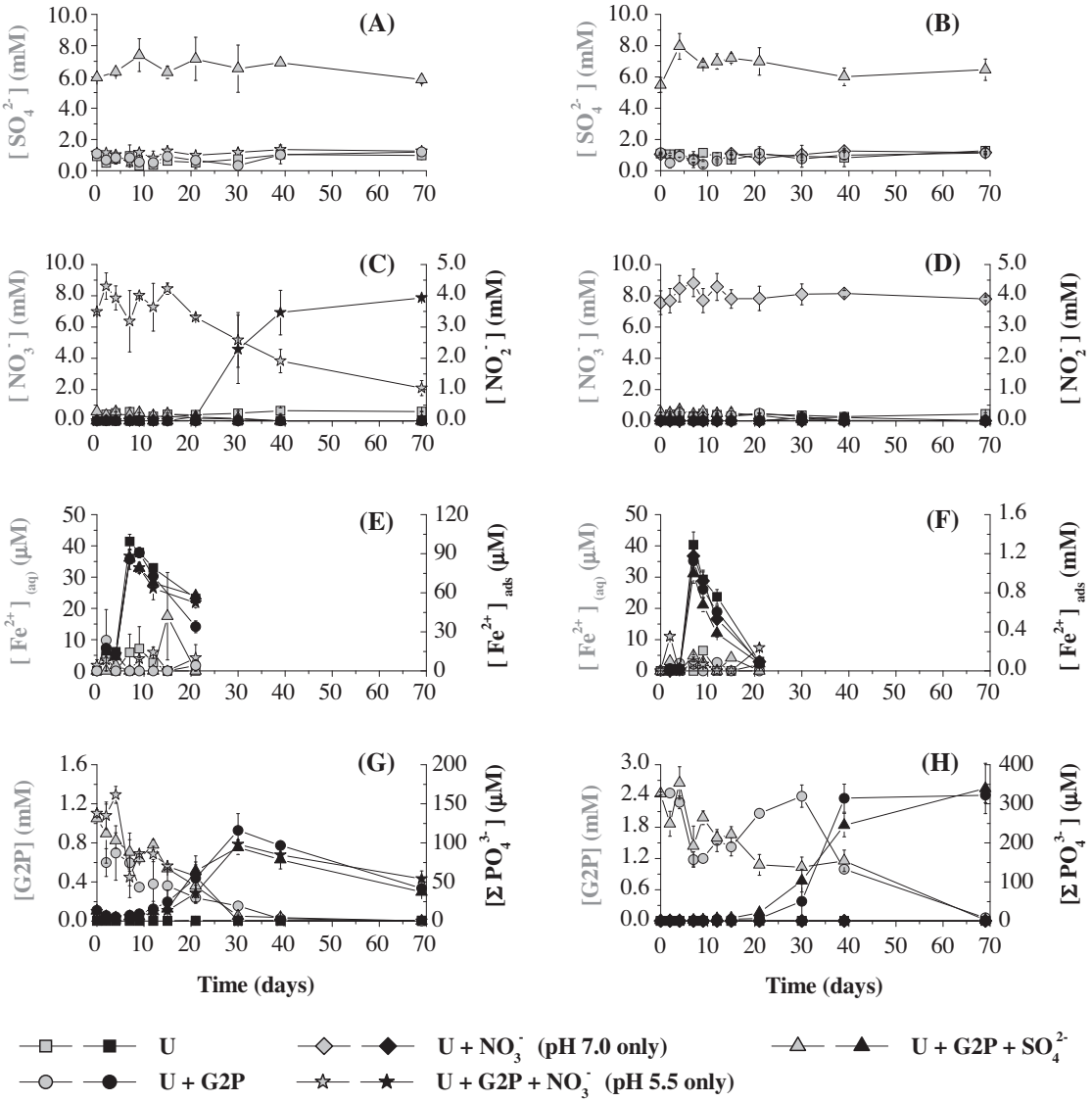

Fig. 1. Evolution of SO_4^{2-} [(A) and (B)], NO_3^- and NO_2^- [(C) and (D)], $Fe^{2+}_{(aq)}$ and adsorbed Fe^{2+} [(E) and (F)], and glycerol-2-phosphate (G2P) and $\sum PO_4^{3-}$ [(G) and (H)] as a function of time in pH 5.5 [(A), (C), (E), and (G)] and pH 7.0 [(B), (D), (F), and (H)] static microcosms amended with 300 μM UO_2^{2+} only; 300 μM UO_2^{2+} and 7 mM NO_3^- (pH 7.0 only); 300 μM UO_2^{2+} and 5 mM G2P; 300 μM UO_2^{2+}, 5 mM G2P, and 7 mM NO_3^- (pH 5.5 only); or 300 μM UO_2^{2+}, 5 mM G2P, and 9.4 mM SO_4^{2-}. Grey symbols represent chemical species on the left axes, while black symbols represent chemical species on the right axes. Error bars represent the range of average reported concentrations between duplicate reactors.

3.2. Solid-phase speciation of uranium and phosphate

A total phosphate concentration of 4.4 ± 0.7 μmol P g^{-1} was extracted in the original sediment prior to phosphate amendment. Not surprisingly, solid phase extractions of sediments revealed higher total extracted phosphate in all G2P-containing reactors than in reactors without G2P (Fig. 3A and B). As expected, phosphate was not detected in the exchangeable fraction (Fig. 3A and B), as phosphate should not exchange with Mg^{2+}. Without G2P, extracted phosphate was primarily concentrated in the residual fraction (Fig. 3A and B). In the presence of G2P, however, the distribution of extracted phosphate shifted towards hydroxylamine- and peroxide-extracted fractions and was not significantly affected by the pH and the presence or type of amended TEA (Fig. 3A and B). As the organophosphate compound was in great excess of uranium in these incubations, the acetate-extractable phosphate fraction, which is representative of uranium–phosphate minerals, was relatively small in all reactors compared to the other treatments (Fig. 3A and B).

The original unamended sediment contained a total concentration of 0.7 ± 0.02 μmol U g^{-1} soil or about 25% of the total extracted uranium after amendments of 300 μM U(VI). The acetate extractable uranium fraction constituted the largest fraction (~60%) of total extracted uranium in all reactor treatments, regardless of the pH (Fig. 4A and B), followed by the hydroxylamine extractable fraction

Table 2
Pseudo-first-order rate constants, k_{obs}, for consumption of NO_3^-, Fe(III), glycerol-2-phosphate (G2P), and dissolved U. For pH 7.0 reactors, only one uranium rate constant was calculated between days 0 and 30. Rate constants reported as N/A represent species that were not present in the given reactor treatment, and rate constants reported as 0 represent species that were not transformed between the initial and final sampling points. Values are reported in units of d^{-1}. Errors represent the standard error of the unweighted slope of linear regressions used to determine rate constants (details in Supplementary material).

Treatment	pH	NO_3^-	Fe(III)	G2P	U
U-amended control	5.5	0	0.66 ± 0.01	N/A	0
	7.0	0	1.36 ± 0.03	N/A	0
G2P-amended reactor	5.5	0.04 ± 0.01	0.62 ± 0.02	0.05 ± 0.01	0.39 ± 0.01[a]
					0.10 ± 0.01[b]
	7.0	0.07 ± 0.03	1.28 ± 0.01	0.10 ± 0.00	0.06 ± 0.01
SO_4^{2-}-amended reactor	5.5	0.04 ± 0.01	0.64 ± 0.01	0.05 ± 0.01	0.39 ± 0.09[a]
					0.11 ± 0.02[b]
	7.0	0.06 ± 0.01	1.38 ± 0.04	0.09 ± 0.02	0.06 ± 0.01
NO_3^--amended reactor	5.5	0.02 ± 0.004	0.54 ± 0.01	0.05 ± 0.02	0.46 ± 0.08[a]
					0.10 ± 0.01[b]
	7.0	0	1.36 ± 0.02	N/A	0

[a] Calculated rate constant between day 0 and day 4 representing the initial uranium removal phase.
[b] Calculated rate constant between day 7 and day 31 representing the secondary removal phase.

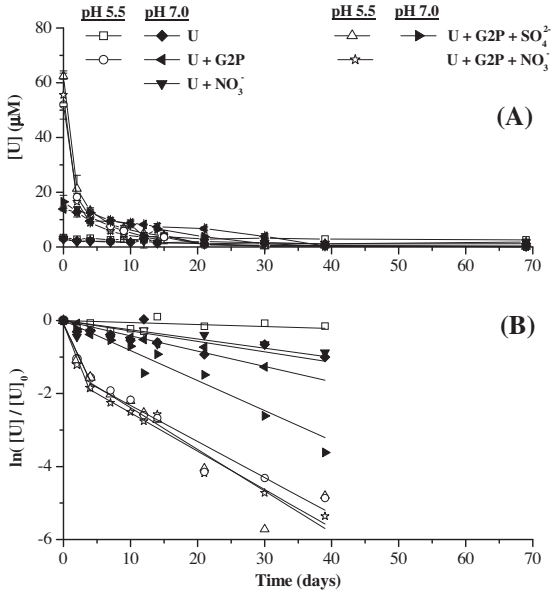

Fig. 2. Evolution of (A) Total dissolved uranium as a function of time in pH 5.5 (open symbols) and pH 7.0 (closed symbols) static microcosms amended with 300 μM UO_2^{2+} only; 300 μM UO_2^{2+} and 7 mM NO_3^- (pH 7.0 only); 300 μM UO_2^{2+} and 5 mM G2P; 300 μM UO_2^{2+}, 5 mM G2P, and 7 mM NO_3^- (pH 5.5 only); or 300 μM UO_2^{2+}, 5 mM G2P, and 9.4 mM SO_4^{2-}. Error bars represent the range of average reported values between duplicate reactors, and uranium standard deviations also include error associated with duplicate measurements. (B) Linearization of total dissolved uranium in all reactors assuming pseudo-first-order with respect to uranium concentration. For pH 5.5 reactors, data points between 0 and 4 days have a distinct linear fit from data points between 7 and 39 days.

(~30%) as the second most abundant. Except for the exchangeable fraction in the pH 5.5 U-amended controls, other fractions did not contribute significantly to total extracted uranium (Fig. 4A and B). Mass-balance on uranium from sequential extractions was respected (within error) in each treatment except for pH 7.0 reactors amended with G2P but no TEA (80.1 ± 11.5%) and pH 7.0 reactors amended with 5 mM NO_3^- but no G2P (116.8 ± 9.9%) (Fig. 4A and B). Further bulk characterization of solid-associated uranium by XAS provided information on the oxidation state and speciation of uranium in each reactor. The normalized and background-subtracted solid phase XANES spectra of samples from each treatment exhibited a uranium L_{III}-edge at ~17,163 eV and a characteristic U(VI) shoulder between 17,188 and 17,200 eV, regardless of pH, indicating U(VI) as the main oxidation state of uranium in these systems (Figs. 5A and 6A). In all pH 5.5 reactors, the k^3-weighted EXAFS fittings confirmed the presence of an axial oxygen shell at 1.80 Å (Fig. 5B and C, Table 3). In addition, two distinct equatorial oxygen shells were evidenced which may be grouped into two subsets based on radial distance (R) from the central uranium atom. The first equatorial oxygen group clustered at approximately 2.30 Å with coordination numbers between 2.3 and 3.5. The second equatorial oxygen group clustered at approximately 2.45 Å with coordination numbers between 1.9 and 3.4. As expected at pH 5.5, carbon from carbonates was not found in the neighborhood of uranium in any reactor. In contrast, Mn and/or Fe shells between 3 and 3.5 Å were necessary in all pH 5.5 reactors to improve the fit. The interatomic distances for sorption complexes between Mn/Fe and U display a wide variety of distances, and these Mn/Fe values fall within the typical range reported elsewhere (Bargar et al., 2000; Webb et al., 2006). Finally, phosphorus shells at ~3.65 Å improved the fit in the G2P-amended reactors without external TEA (day 70) and in the presence of excess sulfate (day 70) and nitrate (day 70).

As observed at pH 5.5, the k^3-weighted EXAFS fittings of pH 7.0 sediments confirmed the presence of an axial oxygen shell at 1.83 Å (Fig. 6B and C, Table 4). Similarly, two distinct equatorial oxygen shells were also observed in all pH 7.0 reactors. The first equatorial oxygen group clustered at approximately 2.25 Å with coordination numbers between 1.4 and 2.0, and the second equatorial oxygen group clustered at approximately 2.42 Å with coordination

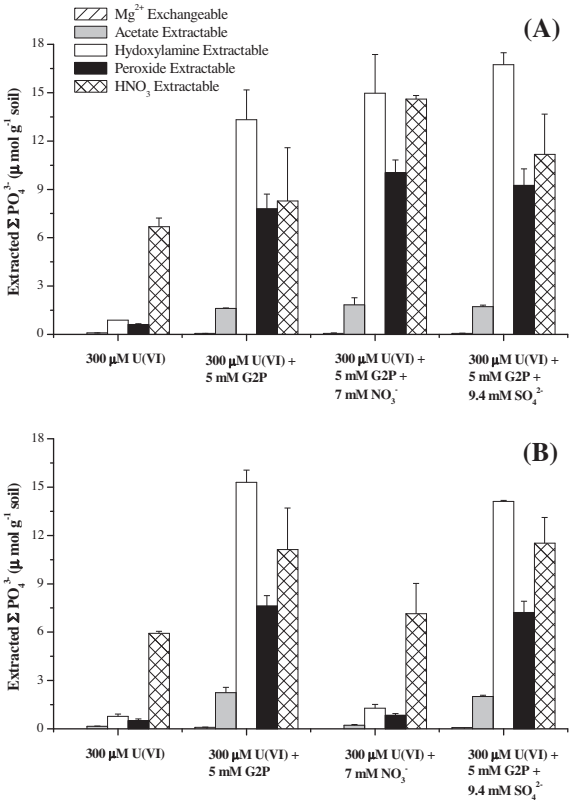

Fig. 3. Solid phase-associated ΣPO_4^{3-} extracted with uranium by the sequential extraction technique of Tessier (1979) from (A) pH 5.5 and (B) pH 7.0 sediments after 70 days of incubation. Bars represent the species extracted during each individual extraction step. A total of 4.4 (±0.7) μmol g^{-1} soil ΣPO_4^{3-} was extracted from the untreated soils. All error bars represent the standard error of the mean calculated from duplicate reactors and duplicate extractions.

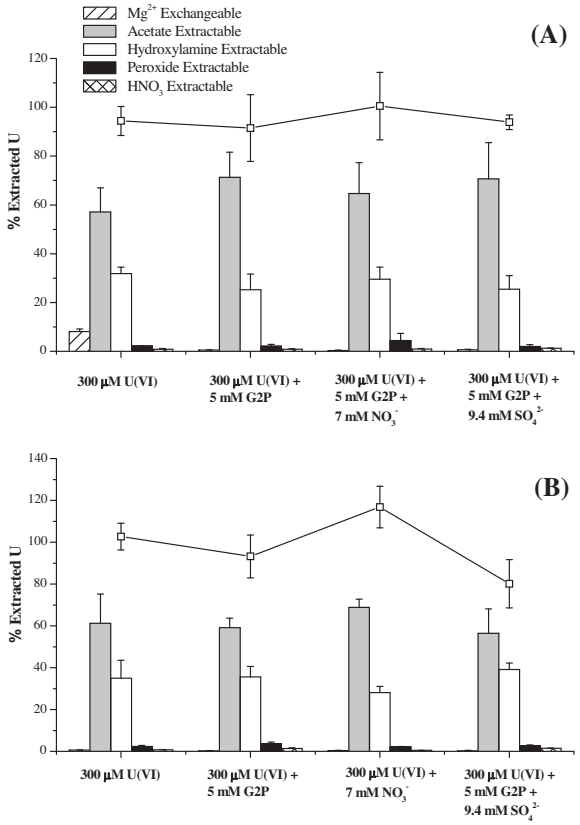

Fig. 4. Solid phase-associated U extracted by the sequential extraction technique of Tessier (1979) from (A) pH5.5 and (B) pH 7.0 sediments after 70 days of incubation. A total of 0.7 (±0) μmol g^{-1} soil U was extracted from the untreated soils. Bars represent percent uranium extracted in each individual extraction step with respect to the total extracted uranium in each treatment. Symbols represent the percent uranium recovered in each reactor with respect to the total mass of extractable uranium. All error bars represent the standard error of the mean calculated from duplicate reactors and duplicate extractions.

numbers between 1.6 and 3.7. As expected at pH 7.0, carbon was needed to improve the fit in the nitrate-amended reactors and the sulfate-amended reactors. Similarly, Mn and/or Fe shells between 3.2 and 3.5 Å were necessary in the pH 7.0 reactors to improve the fit. Finally, phosphorus shells at ~3.65 Å improved the fit in the G2P-amended reactors only.

4. DISCUSSION

Both U(VI) bioreduction and the biomineralization of U(VI)–phosphate minerals are potentially viable approaches to immobilize uranium in contaminated subsurfaces. Bioreduction in low pH soils is typically promoted by buffering the pH to circumneutral values and introducing an electron donor, and U(VI) reduction usually occurs after complete reduction of nitrate (Nyman et al., 2006; Wu et al., 2006b; Madden et al., 2009) and may be concurrent with sulfate or iron reduction (Nyman et al., 2006; Akob et al., 2008; Madden et al., 2009; Cardenas et al., 2010). Biomineralization of U(VI)–phosphate minerals preferentially occurs in low to circumneutral pH conditions in both anaerobic and aerobic environments, provided that organophosphates are available (Beazley et al., 2007, 2009, 2011; Macaskie et al., 1995; Martinez et al., 2007; Montgomery et al., 1995; Shelobolina et al., 2009). Although these processes potentially overlap in reducing conditions, the competition dynamic between adsorption, U(VI)–phosphate biomineralization, and bioreduction has yet to be examined. To determine which anaerobic respiration process is most conducive to uranium removal through U(VI)–phosphate biomineralization and whether bioreduction can compete with biomineralization in G2P-amended sediments, this study investigated the relationship between these competing processes at pH 5.5 and 7.0 in the presence of iron oxides and elevated concentrations of sulfate or nitrate as terminal electron acceptors and G2P as the organophosphate source for U(VI)–phosphate biomineralization.

4.1. Terminal electron acceptor transformations

Although a variety of sulfate-reducing bacteria have been detected in ORFRC wells (Cardenas et al., 2010; Gihring et al., 2011), no evidence of sulfate reduction was

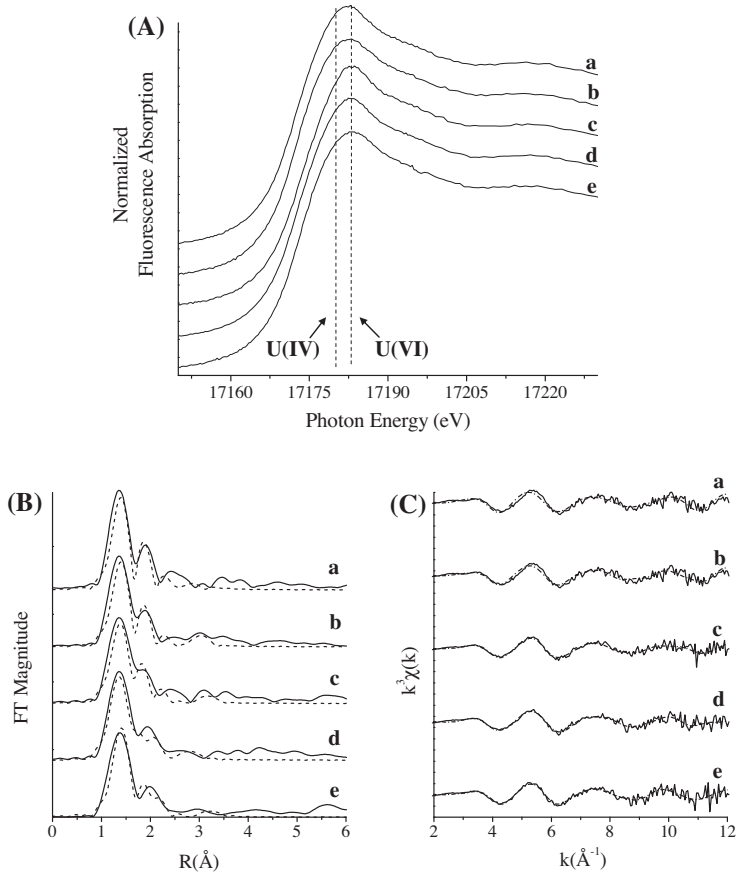

Fig. 5. Uranium (A) XANES, (B) R-space, and (C) *k*-space diagrams of the L_{III}-edge EXAFS obtained from Area 3 sediments of the Oak Ridge Field Research Center incubated anaerobically in static microcosms for 70 days at pH 5.5. Treatments included a (300 μM U + 5 mM G2P, day 0), b (300 μM U + 5 mM G2P, day 70), c (300 μM U + 5 mM G2P + 7 mM NO_3^-, day 70), d (300 μM U + 5 mM G2P + 9.4 mM SO_4^{3-}, day 70), and e (300 μM U, day 70).

observed in any treatment regardless of the presence or absence of G2P and pH conditions (Fig. 1A and B): sulfate concentrations remained steady in all reactors, even after complete removal of nitrate and in the presence of elevated sulfate concentrations; the sediments remained brown, characteristic of the high iron content of ORFRC sediments, throughout the course of the experiment; and sulfide odors were not noticed. These findings are not consistent with past studies conducted with Oak Ridge sediments that observed substantial sulfate reduction after the system pH was raised to between 6.0 and 7.5 (Gu et al., 2005; Wu et al., 2006b; Akob et al., 2008; Kelly et al., 2009; Madden et al., 2009; Kim et al., 2010; Zhang et al., 2010). Electron donor limitations may have prevented sulfate reduction from occurring, as G2P represented the only carbon source added to these incubations. Ambiguous information is available on the ability of sulfate reducers to metabolize or assimilate glycerol, the by-product of G2P hydrolysis. Even though sulfate reduction coupled to glycerol oxidation was observed in acidic sediments conditioned by acid mine drainage (Becerra et al., 2009), sulfate reduction is known to be highly electron donor dependent (Petrie et al., 2003; Madden et al., 2009), suggesting that glycerol may have limited the activity of sulfate-reducing bacteria.

Alternately, the background nitrate concentrations in the present study, reflective of the high nitrate levels at the ORFRC, may have prevented stimulation of sulfate-reducing bacteria. Nitrate-reducing bacteria are diverse and active in ORFRC soils (Spain and Krumholz, 2011), and a subset of the nitrate reducers that are metabolically active include members of the genera *Burkholderia*, *Ralstonia*, *Castellaniella*, *Herbaspirillum*, *Dechloromonas*, *Zooglea*, *Rhodanobacter*, *Rhizobiaceae*, *Sphingomonas*, *Magnetospirillum*, and *Paenibacillus* (Akob et al., 2007; Mohanty et al., 2008; Green et al., 2010, 2012). In addition, *Rahnella* sp. Y9602, a phosphatase-positive metal-resistant bacterium isolated from ORFRC soils (Martinez et al., 2006), is able to reduce nitrate anaerobically while promoting biomineralization of U(VI)–phosphate minerals (Beazley et al., 2009). The results of the present study confirm that G2P addition is sufficient to stimulate nitrate reduction by indigenous nitrate reducing bacteria of ORFRC sediments in varied pH conditions and variable nitrate concentrations (Fig. 1C and D). The higher pseudo first-order rate constant at pH 7.0 compared to pH 5.5 (Table 2) indicates that nitrate reduction was more efficient at circumneutral pH, which is consistent with previous findings at the ORFRC (Shelobolina et al., 2003; Istok et al., 2004;

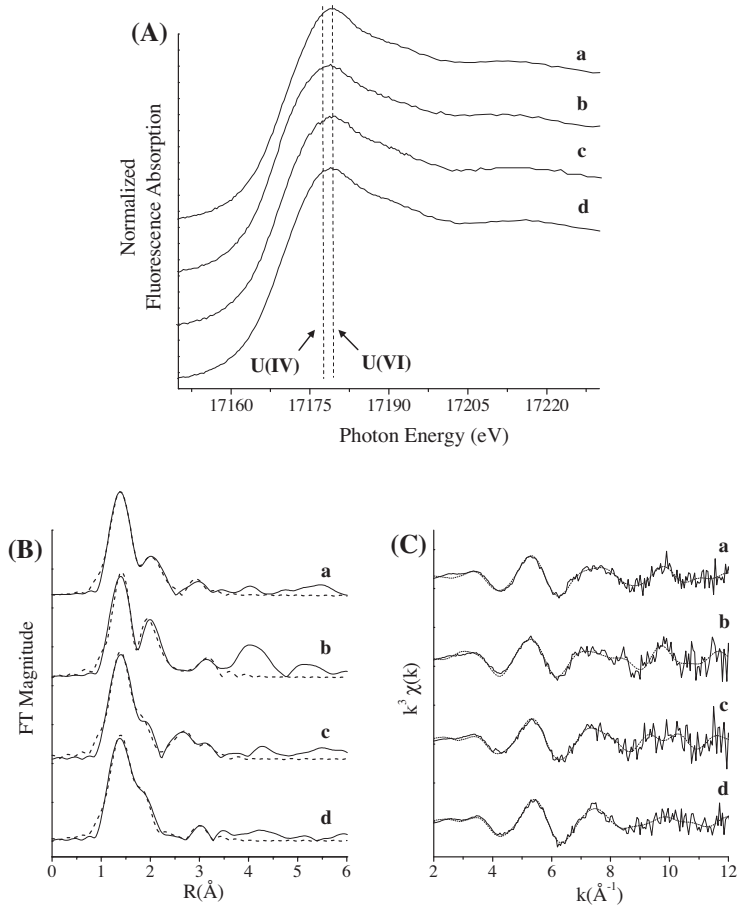

Fig. 6. Uranium (A) XANES, (B) R-space, and (C) *k*-space diagrams of the L_{III}-edge EXAFS obtained from Area 3 sediments of the Oak Ridge Field Research Center incubated anaerobically in static microcosms for 70 days at pH 7.0. Treatments included a (300 μM U, 70 days), b (300 μM U + 7 mM NO_3^-,70 days), c (300 μM U + 5 mM G2P,70 days), and d (300 μM U + 5 mM G2P + 9.4 mM SO_4^{3-}, 70 days).

Edwards et al., 2007). Simultaneously, only ephemeral nitrite accumulation was observed in incubations amended with G2P only and both G2P and sulfate regardless of pH (Fig. 1C and D), likely due to further reduction of nitrite to other denitrification products or ammonia during dissimilatory nitrate reduction to ammonia (DNRA) (Herbert, 1999). In turn, 4 mM NO_2^- accumulated in pH 5.5 nitrate-amended reactors (Fig. 1C), and comparison of nitrate reduction rates (-180.9 ± 11.6 μM d^{-1}) and net nitrite production rates at pH 5.5 (157.3 ± 4.7 μM d^{-1}) suggests denitrification or DNRA removed nitrite from this reactor at a rate of -23.6 ± 12.5 μM d^{-1}.

The accumulation of high NO_2^- concentrations in the pH 5.5 nitrate-amended reactors may also have had a toxic effect on denitrifying bacteria that is reflected in a decrease in the pseudo-first-order rate constant for nitrate reduction in nitrate-amended reactors compared to G2P-amended and sulfate-amended reactors (Table 2). The nitrite toxicity effect is well documented and is evidenced in a wide variety of microorganisms. Proposed mechanisms include an increase in the permeability of the cytoplasmic membrane (Sijbesma et al., 1996) and the disruption of proton translocation stoichiometry (Rake and Eagon, 1980). In addition, elevated levels of nitrite have been shown to interfere with denitrification pathways, a phenomenon that is known to be exaggerated in anaerobic conditions (Bollag and Henninger, 1978; Meijer et al., 1979). These findings suggest that the accumulation of NO_2^- in the pH 5.5 nitrate-amended reactors may have resulted from the toxicity of NO_2^- on nitrite-reducing bacteria, while the relatively minimal NO_2^- concentrations detected in other incubations were likely not significant to affect nitrite-reducing bacteria.

Iron reduction was not significantly inhibited by elevated nitrate concentrations (Fig. 1C–F) in contrast to what is known about the inhibitory effect of nitrate on iron reduction (Dichristina, 1992; Senko et al., 2002; Finneran et al., 2002a,b). In addition, iron reduction was unaffected by the presence of G2P (Fig. 1E and F). However, a significant inhibition on iron reduction was apparent at pH 5.5 (Fig. 1E), consistent with previous findings demonstrating that microbial growth is impacted in low pH conditions (Edwards et al., 2007). As Fe^{2+} production preceded nitrate removal and production of nitrite, chemical reduction of Fe^{3+} coupled to reoxidation of nitrite was likely not significant, and the observed production of Fe^{2+} was likely due to microbially-mediated G2P-independent iron reduction in the presence of nitrate (Fig. 1C–F). These observations suggest that iron-reducing bacteria present at the ORFRC

Table 3
Fitting parameters for U L_{III}-edge EXAFS derived using SIXPACK (Webb, 2005) in pH 5.5 reactors. Treatments include a (300 μM U, day 70), b (300 μM U + 5 mM G2P, day 0), c (300 μM U + 5 mM G2P, day 70), d (300 μM U + 5 mM G2P + 7 mM NO_3^-, day 70), and e (300 μM U + 5 mM G2P + 9.4 mM SO_4^{3-}, day 70). *N* represents U-ligand coordination number, *R*(Å) represents U-ligand distance.

Path	Treatment	*N*	*R*(Å)	σ^2	*R* factor	ΔE_0
$U–O_{ax}$	a	2.00	1.80 ± 0.01	0.002 ± 0.001	0.0556	11.4 ± 2.92
	b	2.00	1.79 ± 0.01	0.001 ± 0.000	0.0399	9.63 ± 2.01
	c	2.00	1.80 ± 0.01	0.002 ± 0.001	0.0367	9.99 ± 2.29
	d	2.00	1.79 ± 0.01	0.002 ± 0.001	0.0522	8.22 ± 2.87
	e	2.00	1.76 ± 0.01	0.002 ± 0.001	0.0345	2.82 ± 3.07
$U–O_{eq\ 2.30}$	a	2.34 ± 0.65	2.30 ± 0.03	0.003		
	b	3.49 ± 0.55	2.35 ± 0.01	0.003		
	c	3.01 ± 0.55	2.34 ± 0.02	0.003		
	d	3.14 ± 0.63	2.30 ± 0.02	0.003		
	e	2.94 ± 0.58	2.22 ± 0.02	0.003		
$U–O_{eq\ 2.45}$	a	2.60 ± 0.75	2.46 ± 0.03	0.003		
	b	2.14 ± 0.71	2.53 ± 0.02	0.003		
	c	1.86 ± 0.70	2.52 ± 0.03	0.003		
	d	2.33 ± 0.76	2.47 ± 0.03	0.003		
	e	3.44 ± 0.62	2.39 ± 0.02	0.003		
U–Mn/Fe	a	0.20 ± 0.39	3.54 ± 0.01	0.003		
	b	0.32 ± 0.29	3.29 ± 0.05	0.003		
	c	0.36 ± 0.54	3.41 ± 0.06	0.003		
	d	0.31 ± 1.99	3.52 ± 0.27	0.003		
	e	0.40 ± 0.28	3.28 ± 0.04	0.003		
U–P	a					
	b					
	c	0.17 ± 1.11	3.62 ± 0.33	0.003		
	d	0.57 ± 2.32	3.60 ± 0.40	0.003		
	e	0.75 ± 0.71	3.72 ± 0.06	0.003		

Errors are given for values which were allowed to float.
No error means value was fixed or calculated from other parameters.

may be active in nutrient- and electron donor-limited environments when nitrate-reducing bacteria remain dormant.

The rapid rise and decrease of adsorbed Fe^{2+} not balanced by accumulation of dissolved Fe^{2+} in all reactors regardless of pH (Fig. 1E and F) suggests that Fe^{2+} was not desorbed via an ion exchange process and instead precipitated as a distinct mineral. XANES spectra confirmed the bulk oxidation state of uranium as U(VI) in all reactors (Figs. 5A and 6A), suggesting the chemical oxidation of sorbed Fe^{2+} by U(VI) (Liger et al., 1999) was likely not significant at pH 7.0 or inhibited at pH 5.5. As thermodynamic calculations predicted little adsorption of Fe^{2+} at pH 5.5 (Table 5), the observed adsorption of Fe^{2+} in all reactor treatments may have been driven by formation of ternary $\equiv Fe—OPO_3—Fe^+$ complexes with iron oxides. These complexes are well known to occur under both pH conditions and are thought to be precursors to the surface precipitation of iron phosphate minerals even in undersaturated conditions (Li and Stanforth, 2000; Ler and Stanforth, 2003), but they were not included in the thermodynamic model. Thus, despite the fact that equilibrium calculations predict undersaturation of vivianite [$Fe_3(PO_4)_2$] at both pHs in the conditions of the incubations (Table 5), the decrease in total Fe^{2+} coinciding with the accumulation of inorganic phosphate in solution (Fig. 1E–H) could be explained by the formation of ternary iron phosphate complexes and subsequent surface-catalyzed precipitation of vivianite. This process should be investigated in future studies.

4.2. Organophosphate hydrolysis

Incubations in the presence of G2P clearly illustrate that organophosphate hydrolysis is significant in reducing conditions (Fig. 1G and H) and stimulates anaerobic respiration of nitrate (Fig. 1C and D) compared to otherwise identical control incubations without G2P. The distribution of phosphate extracted simultaneously with uranium from the solid phase at the end of the incubations demonstrates that phosphate exists primarily in highly recalcitrant phases in the absence of organophosphate (Fig. 3A and B), suggesting that anaerobic respiration is limited by the availability of phosphorus in these conditions. In contrast, the distribution of solid-phase associated phosphate shifts towards more reactive phases in the presence of G2P (Fig. 3A and B). These findings imply the supply of labile organic carbon (i.e. glycerol) or phosphate to support the metabolism and growth of the indigenous microbial community represents the driving force for G2P hydrolysis. Previous studies have demonstrated glycerol oxidation coupled to iron (Petrie et al., 2003), sulfate (Qatibi et al., 1991), and uranium (Madden et al., 2007) reduction, while

Table 4
Fitting parameters for U L_{III}-edge EXAFS derived using SIXPACK (Webb, 2005) in pH 7.0 reactors. Treatments include a (300 μM U, day 70), b (300 μM U + 7 mM NO_3^-, day 70), c (300 μM U + 5 mM G2P, day 70), and d (300 μM U + 5 mM G2P + 9.4 mM SO_4^{3-}, day 70). *N* represents U-ligand coordination number, *R*(Å) represents U-ligand distance.

Path	Treatment	*N*	*R*(Å)	σ^2	*R*factor	ΔE_0
U–O_{ax}	a	2.00	1.87 ± 0.01	0.008 ± 0.002	0.0252	13.9 ± 3.1
	b	2.00	1.86 ± 0.04	0.006 ± 0.003	0.0436	10.4 ± 3.6
	c	2.00	1.85 ± 0.03	0.005 ± 0.003	0.0555	7.45 ± 3.9
	d	2.00	1.78 ± 0.01	0.007 ± 0.001	0.0128	2.34 ± 1.4
U–$O_{eq\ 2.30}$	a	1.37 ± 0.49	2.30 ± 0.03	0.003		
	b	1.35 ± 1.6	2.28 ± 0.10	0.003		
	c	2.05 ± 2.5	2.25 ± 0.06	0.003		
	d	1.72 ± 0.31	2.20 ± 0.02	0.003		
U–$O_{eq\ 2.45}$	a	1.64 ± 0.58	2.46 ± 0.02	0.003		
	b	2.65 ± 2.19	2.44 ± 0.07	0.003		
	c	3.73 ± 3.22	2.42 ± 0.04	0.003		
	d	1.96 ± 0.37	2.35 ± 0.02	0.003		
U–C	a					
	b	1.19 ± 1.39	2.87 ± 0.06	0.003		
	c					
	d	1.67 ± 0.62	2.95 ± 0.03	0.003		
U–Mn/Fe	a	0.27 ± 0.14	3.43 ± 0.03	0.003		
	b	0.49 ± 0.42	3.47 ± 0.06	0.003		
	c	0.30 ± 0.43	3.18 ± 0.07	0.003		
	d	0.43 ± 0.16	3.24 ± 0.02	0.003		
U–P	a					
	b					
	c	1.02 ± 1.14	3.61 ± 0.06	0.003		
	d	0.62 ± 0.35	3.69 ± 0.03	0.003		

Errors are given for values which were allowed to float.
No error means value was fixed or calculated from other parameters.

organophosphate hydrolysis by bacterially-derived phosphatase enzymes is thought to provide inorganic phosphorus either for nutrient assimilation or as a heavy-metal detoxification mechanism (Macaskie et al., 1992). As uranium reduction was not favored in these incubations and as G2P consumption in reactors amended with G2P was so intense (1.2–2.4 mM, Fig. 1G and H) compared to the availability of uranium (300 μM) in these sediments, G2P was likely hydrolyzed by bacterially-derived phosphatases produced due to phosphorus or carbon limitations. In addition, G2P hydrolysis may have been enhanced at pH 7.0 (Table 2) in response to the decrease in adsorption of G2P onto iron oxides due to the repulsion between partially deprotonated iron oxides and totally deprotonated G2P at that pH. As nitrate reduction is clearly promoted by the presence of G2P in solution compared to the unamended control (Fig. 1D), the decrease in G2P adsorption and associated increase in G2P hydrolysis at pH 7.0 may have also promoted the increase in the pseudo-first order rate constants for nitrate reduction observed at circumneutral pH in the incubations amended with G2P compared to at pH 5.5 (Table 2). Indeed, factoring out initial concentration of G2P from the pseudo-first order rate constants reveals similar rate constants for nitrate reduction at both pH 5.5 and 7.0 (not shown). Finally, the disparity between G2P consumption and phosphate production in solution in all G2P-containing reactors (Fig. 1G and H) indicates the existence of a significant phosphate removal mechanism other than U(VI)–phosphate biomineralization. Thermodynamic modeling suggests ~80% phosphate removal through adsorption in these incubations at both pH 5.5 and 7.0 (Table 5), and solid-phase extractions (Fig. 3A and B) confirm large quantities of phosphate associated with iron and manganese oxides in these sediments. Thus, sorption was likely primarily responsible for phosphate removal with less significant contributions from precipitation of U(VI)–phosphate minerals and assimilation by the natural microbial community.

4.3. Fate of uranium

Although each treatment received a 300 μM U(VI) amendment, approximately 20% of uranium at pH 5.5 and less than 5% at pH 7.0 remained in solution initially in each reactor (Fig. 2A). As ~95% of uranium removal between pH 5.5 and 7.0 is achieved through sorption in ORFRC soils (Barnett et al., 2000) and inorganic phosphate was initially unavailable to support U(VI) removal through the biomineralization of U(VI)–phosphate minerals, the initial uranium removal observed in all reactors can be attributed to adsorption. Important sorbents in ORFRC sediments include predominantly ferric and alumi-

Table 5
Predicted solution equilibrium and solid phase saturation indices using MINEQL+ (Schecher and McAvoy, 2001) in pH 5.5 and 7.0 incubations assuming 5 mM ΣPO_4^{3-} was produced by G2P hydrolysis. Solution concentrations are reported in percent of total species. Each treatment (Table 1) was modeled using the maximum measured total Fe^{2+} concentration and initial conditions as input for all other species. A double layer sorption model onto amorphous Fe-oxide (3.2 g/L, 600 m^2/g surface area) was included in the calculations. Unless otherwise noted, log K values are as reported in Schecher and McAvoy (2001).

Species	Log *K*	Treatment			
		U-amended control	G2P-amended reactor	SO_4^{2-}-amended reactor	NO_3^--amended reactor
pH 5.5					
UO_2^{2+}					
$UO_2CO_{3(aq)}$	9.94[a]	25.9%	0.1%	0.0%	0.1%
Fe(wk)OH–$UO_2(OH)_2$	−6.28[b]		0.0%	0.0%	0.0%
Fe(st)OH–$UO_2(OH)_2$	−2.57[b]		0.7%	0.3%	0.4%
Others	–	6.8%	–	–	–
PO_4^{3-}					
Fe(wk)H_2PO_4	31.29	–	44.7%	48.4%	48.4%
Fe(wk)HPO_4^-	25.39	–	45.5%	41.6%	41.6%
Others (Autunite)	–	–	9.9%	10.0%	10.0%
Fe^{2+}				9.8%	
Fe^{2+}		91.3%	93.4%	57.5%	94.7%
Fe(st)OH–$Fe(OH)^+$	−0.95[c]	0.0%	3.60%	2.70%	2.80%
Fe(wk)–$Fe(OH)^+$	−2.98[c]	6.8%	1.50%	1.10%	1.10%
Others	–	1.9%	1.5%	1.5%	1.4%
Solid phase					
Schoepite	−5.2[d]	−0.981	−3.48	−3.84	−3.70
Na–Autunite	47.4	−28.4	0 (99.2% U)	0 (99.7% U)	0 (99.5% U)
Ca–Autunite	44.7[d]	−32.05	−3.51	−4.16	−3.88
K–Autunite	22.73[e]	−28.64	−0.19	−0.72	−0.44
Vivianite	36.0[f]	−40.62	−7.10	−6.99	−6.98
Siderite	10.24[g]	−3.24	−3.20	−3.25	−3.24
pH 7.0					
UO_2^{2+}					
$UO_2(CO_3)_2^{-2}$	16.61[a]	11.3%	0.1%	0.1%	12.3%
$CaUO_2(CO_3)_3^{-2}$	27.18[h]	28.4%	0.5%	0.2%	27.8%
$Ca_2UO_2(CO_3)_3^0$	30.7[h]	6.4%	0.2%	0.1%	6.0%
Fe(st)OH–$UO_2(OH)_2$	−2.57[b]	47.3%	0.0%	0.0%	47.3%
Others	–	6.6%	–	–	6.6%
PO_4^{3-}					
Fe(wk)H_2PO_4	31.29	–	23.7%	22.8%	–
Fe(wk)HPO_4^-	25.39	–	61.9%	62.6%	–
Others	–	–	14.4%	14.6%	–
Fe^{2+}					
Fe^{2+}		4.4%	38.2%	34.8%	4.5%
Fe(wk)–$Fe(OH)^+$	−2.98[c]	71.3%	47.8%	40.5%	71.1%
Fe(st)OH–$Fe(OH)^+$	−0.95[c]	22.3%	7.00%	8.60%	22.4%
Fe(wk)–$Fe(OH)_2$	−11.55[c]	1.9%	1.30%	1.10%	1.9%
Others	–	0.1%	5.7%	15.0%	0.1%
Solid phase					
Schoepite	−5.2[d]	−2.32	−4.30	−4.50	−2.32
Na–Autunite	47.4	−32.21	0 (99.2% U)	0 (99.6% U)	−32.00
Ca–Autunite	44.7[d]	−35.95	−3.65	−4.29	−35.98
K–Autunite	22.73[e]	−32.42	−0.19	−0.72	−32.45
Vivianite	36.0[f]	−39.70	−0.63	−0.97	−39.72
Siderite	10.24[g]	−2.35	−1.34	−1.44	−2.36

[a] Guillaumont et al. (2003).
[b] Waite et al. (1994).
[c] Appelo et al. (2002).
[d] Langmuir (1997).
[e] Van Haverbeke et al. (1996).
[f] Nriagu (1972).
[g] Singer and Stumm (1970).
[h] Dong and Brooks (2006).

num oxides (Brooks, 2001), which display a pH_{zpc} around 7.0 (Hsi and Langmuir, 1985; Stumm and Morgan, 1996; Langmuir, 1997), and to a lesser extent manganese oxides (Barnett et al., 2000), which display a pH_{zpc} ranging between 1.3 and 7.3 (Langmuir, 1997). Aluminum oxides, however, are less likely to be involved in the removal of uranium at pH greater than 4.0 in the presence of iron oxides (Zheng et al., 2003). Indeed, bulk uranium EXAFS of both pH 5.5 and pH 7.0 reactors demonstrate uranium associated with Mn and/or Fe phases (Tables 3 and 4). At pH 5.5, U(VI) carries a positive (UO_2^{2+}) or neutral ($UO_2CO_{3(aq)}$) charge (Table 5), making it less likely to adsorb to positively charged soils than negatively charged G2P or orthophosphates which strongly compete for soil sorption sites, especially given their high concentration. In fact, thermodynamic modeling predicts ~70% adsorption of U(VI) at pH 5.5 in the absence of phosphate (U-control) as compared to ~1% adsorption in the presence of 5 mM phosphate from organophosphate hydrolysis (G2P-treatments) (Table 5). At pH 7.0, U(VI) is primarily present as neutral [$Ca_2UO_2(CO_3)_3$] and negatively charged species ($CaUO_2(CO_3)_3^{2-}$) (Table 5), and G2P is totally deprotonated. As evidenced by the initial twofold increase in dissolved G2P at pH 7.0 compared to pH 5.5 (Fig. 1D), G2P adsorbs less efficiently at pH 7.0 when surface sites shift towards more negative values. Thus, the decreased sorption of G2P allows for more complete sorption of U(VI) species and is reflected in the fourfold decrease in aqueous uranium at pH 7.0 versus pH 5.5 initially (Fig. 2A). In a similar fashion, the initial adsorption of U(VI) at pH 7.0 is much higher in the absence (U-control) than in the presence of organophosphate.

Examination of the removal of uranium as a function of time reveals interesting features. At pH 5.5, two kinetically-controlled uranium removal phases are observed in all G2P-containing reactors (Fig. 2) in agreement with previous studies that demonstrated rapid adsorption of U(VI) to ferrihydrite within the first few hours of equilibration at pH 5.0 is followed by a secondary removal phase that lasts several days (Waite et al., 1994). The first removal phase that occurs between 0 and 4 days could be attributed to the diffusion-limited sorption of uranium in the crystal lattice of minerals or pores of the soil matrix (Davis and Kent, 1990; Waite et al., 1994), as during that time period hydrolysis of G2P was not significant as indicated by the relatively constant concentration of G2P in solution and the lack of production of inorganic phosphates (Fig. 1G). The second phase that occurs between 4 and 40 days is attributed to the precipitation of uranium phosphate controlled by the hydrolysis of G2P, as previously demonstrated in pure cultures incubations with an organism isolated from the same site (Beazley et al., 2007, 2009) and supported by the decrease in G2P, the simultaneous production of dissolved phosphate after a small phase lag (Fig. 1G), and the thermodynamic calculations that predict precipitation of almost all uranium as autunite mineral (Table 5). In pH 7.0 reactors containing G2P, only one uranium removal phase was observed (Fig. 2), suggesting that uranium carbonate complexes, the dominant form of dissolved uranium in the absence of inorganic phosphate at that pH (Table 5), do not promote the diffusion-limited removal process observed in the pH 5.5 incubations. The slightly lower pseudo-first-order rate constants calculated for the removal of uranium at pH 7.0 compared the second uranium removal phase at pH 5.5 (Table 2) may be attributed to the stabilization of uranium in solution by carbonates. Overall, these data suggest that similar U(VI) removal mechanisms were ongoing in the pH 7.0 incubations. Indeed, thermodynamic calculations predict the majority of uranium is precipitated under the form of autunite minerals (Table 5).

Bioreduction is a commonly observed removal pathway for U(VI) in anaerobic conditions. In this study, however, XANES data did not show evidence of U(VI) reduction regardless of pH, even after complete nitrate removal (Figs. 5A and 6A). These findings suggest that U(VI) reduction was inhibited in these incubations. Similar results were observed in both pure culture systems and sediment microcosms. Both manganese (Liu et al., 2002) and ferrihydrite (Wielinga et al., 2000) were shown to inhibit uranium reduction by acting as competitive terminal electron acceptors in pure cultures, while calcium was shown to inhibit reduction of U(VI) in pure cultures through the formation of ternary $Ca–UO_2–CO_3$ complexes which are less energetically favorable terminal electron acceptors than free uranyl ions (Brooks et al., 2003). In addition, uranium reduction in ORFRC sediments commonly occurs concurrently with sulfate reduction (Nyman et al., 2006; Wu et al., 2006b; Luo et al., 2007; Akob et al., 2008; Madden et al., 2009; Cardenas et al., 2010; Kostka and Green, 2011). Although the exact mechanism of this coupling is unknown, it has recently been suggested that the observed U(VI) reduction is driven by the formation of iron sulfides and subsequent sulfide-catalyzed chemical reduction of U(VI) to U(IV) (Hyun et al., 2012). As no sulfate reduction was observed in the present incubations and $Ca–UO_2–CO_3$ aqueous species are predicted to dominate the speciation of U(VI) in solution (Table 5), it is unlikely that uranium reduction occurred over the experimental time scale of 70 days. Finally, the chemical oxidants NO_2^-, Fe(III), and/or possibly MnO_2, which can re-oxidize uraninite in reducing conditions (Fredrickson et al., 2002; Senko et al., 2002, 2005a,b; Wan et al., 2005; Moon et al., 2007), were present in great excess in these incubations suggesting any reduced uranium would have been destabilized.

The biomineralization of U(VI)–phosphate minerals represents an alternative U(VI) removal mechanism and has been demonstrated in both pure culture (Macaskie et al., 1995; Montgomery et al., 1995; Beazley et al., 2007; Martinez et al., 2007) and soil studies (Shelobolina et al., 2009; Beazley et al., 2011). The observed G2P consumption and subsequent production of inorganic phosphate support the hypothesis that U(VI)–phosphate biomineralization is an important contributor to U(VI) removal in these experiments, and the lack of observed uranium reduction is indicative of the formation of more stable U(VI)–phosphate minerals (Beazley et al., 2007, 2011; Shelobolina et al., 2009). In all incubations, solid-phase extractions revealed uranium primarily associated with phosphate minerals (acetate extractable fraction) and bound to iron/manganese oxides (hydroxylamine extracted) (Fig. 4A and B). While

this was expected for G2P-containing reactors, uranium in the U-amended controls was also found in the acetate extractable fraction. This discrepancy is likely due to precipitation of schoepite during the pH 7.0 $MgCl_2$ extraction step designed to desorb loosely bound uranium (not shown) and does not reflect actual precipitation of U(VI)–phosphate minerals in reactors unamended with G2P. Thermodynamic calculations and EXAFS data support the formation of U–P minerals at both pH 5.5 and 7.0 (Tables 3–5). Equilibrium calculations predict 99% of uranium precipitates under the form of autunite minerals at both pHs (Table 5), even when uranium phosphate ternary complexes are included in the model. Following incubation for 70 days at pH 5.5 and 7.0, the fit for all G2P-containing reactors was improved by the inclusion of a U–P scattering path to the EXAFS fitting (Table 4 and Fig. 5B). In contrast, the fit was not improved by the addition of a U–P EXAFS scattering path for the sample taken from G2P-amended reactors prior to incubation, supporting the hypothesis that the initial uranium removal by adsorption was followed by the biomineralization of U(VI)–phosphate minerals.

These findings have important implications for the design and implementation of uranium remediation strategies in contaminated subsurface environments. First, U(VI) biomineralization promoted by G2P hydrolysis appears to outcompete U(VI) bioreduction in nitrate- and iron-rich environments. Almost complete uranium removal may be achieved in high nitrate conditions found at some radionuclide-contaminated sites without the preconditioning steps (i.e. nitrate removal and pH adjustments) required to promote U(VI) bioreduction (Wu et al., 2006a). Eliminating these conditioning steps may help minimize the cost of remediation. In contrast, if sulfate-reducing microorganisms are not stimulated by organophosphate addition, nor involved in organophosphate hydrolysis as suggested by the findings of this study, sulfate-reducing conditions promoted by endogenous electron donors should lead to formation of uraninite and other U(IV) mineral products. Finally, the low phosphate levels in most subsurface environments are likely to favor phosphatase activity by native subsurface microbial populations. The fact that such activity occurs under both aerobic (Shelobolina et al., 2009; Beazley et al., 2011) and anaerobic conditions (this study), coupled to the fact that uranium phosphate minerals are highly stable in a wide range of redox conditions compared to U(IV) minerals, indicate that biomineralization of U(VI)–phosphate minerals may be particularly useful at contaminated sites subject to fluctuating redox conditions.

5. CONCLUSIONS

The instability of uraninite, even under reducing conditions, generates the need for an alternative bioremediation strategy to decrease the solubility of uranium in contaminated environments. Biomineralization of U(VI)–phosphate minerals, a possible complementary technique to bioreduction, has been shown to be applicable in both reducing and oxidizing environments, and the ability of ORFRC microbial isolates to metabolize G2P in aerobic conditions has been demonstrated. In this study, the competition dynamic between U(VI) bioreduction, U(VI)–phosphate biomineralization, and adsorption in the presence of G2P and alternate terminal electron acceptors was studied in anaerobically-maintained ORFRC contaminated sediments at two different pHs to determine which respiratory process is promoted by G2P in these sediments and its influence on the fate of uranium.

The addition of G2P to ORFRC Area 3 sediments was sufficient to stimulate reduction of nitrate at both pH 5.5 and 7.0 but not sulfate, even after complete removal of nitrate, suggesting the lack of a suitable electron donor for sulfate-reducing bacteria in these incubations. Although more efficient at pH 7.0, anaerobic respiration of iron oxides occurred at both pHs, even in the presence of high nitrate concentrations, and appeared to be unaffected by the addition of G2P. In turn, nitrate reduction depended on G2P hydrolysis and was enhanced at circumneutral pH, suggesting that G2P availability in the dissolved phase may control the intensity of anaerobic nitrate respiration in these sediments. High nitrate reduction rates simultaneously impacted nitrite-reducing microorganisms significantly, likely via accumulation of the toxic nitrite in solution. Hydrolysis of G2P was much more significant than the availability of uranium at both pHs, suggesting that the hydrolysis of organophosphate in these sediments was activated by phosphate or carbon limitations rather than a uranium detoxification mechanism. Finally, almost complete removal of uranium through a combination of adsorption and precipitation of uranium phosphate minerals was observed at both pHs. Overall, the results of this study not only suggest that biomineralization of U(VI)–phosphate minerals may be complementary to bioreduction, but also that U(VI)–phosphate biomineralization may be preferable to bioreduction in certain environments due to its utility in a wide range of chemical and redox conditions.

ACKNOWLEDGMENTS

This research was supported by the Office of Science (BER), US Department of Energy Grant No. DE-FG02-04ER63906. Portions of this research were carried out at the Stanford Synchrotron Radiation Lightsource, a national user facility operated by Stanford University on behalf of the US Department of Energy, Office of Basic Energy Sciences. The SSRL Structural Molecular Biology Program is supported by the Department of Energy, Office of Biological and Environmental Research, and by the National Institutes of Health, National Center for Research Resources, Biomedical Technology Program. We thank Dave Watson of Oak Ridge National Laboratory for providing ORFRC sediment cores and Eric Roden for providing thermodynamic stability constants of glycerol phosphate adsorption onto iron oxides.

APPENDIX A. SUPPLEMENTARY DATA

Supplementary data associated with this article can be found, in the online version, at http://dx.doi.org/10.1016/j.gca.2012.12.037.

REFERENCES

Akob D. M., Mills H. J., Gihring T. M., Kerkhof L., Stucki J. W., Anastacio A. S., Chin K. J., Kusel K., Palumbo A. V., Watson D. B. and Kostka J. E. (2008) Functional diversity and electron donor dependence of microbial populations capable of U(VI) reduction in radionuclide-contaminated subsurface sediments. *Appl. Environ. Microbiol.* **74**, 3159–3170.

Akob D. M., Mills H. J. and Kostka J. E. (2007) Metabolically active microbial communities in uranium-contaminated subsurface sediments. *FEMS Microbiol. Ecol.* **59**, 95–107.

Allen P. G., Shuh D. K., Bucher J. J., Edelstein N. M., Palmer C. E. A., Silva R. J., Nguyen S. N., Marquez L. N. and Hudson E. A. (1996) Determinations of uranium structures by EXAFS: schoepite and other U(VI) oxide precipitates. *Radiochim. Acta* **75**, 47–53.

Ankudinov A. L., Ravel B., Rehr J. J. and Conradson S. D. (1998) Real-space multiple-scattering calculation and interpretation of X-ray-absorption near-edge structure. *Phys. Rev. B* **58**, 7565.

Appelo C. A. J., Van der Weiden M. J. J., Tournassat C. and Charlet L. (2002) Surface complexation of ferrous iron and carbonate on ferrihydrite and the mobilization of arsenic. *Environ. Sci. Technol.* **36**, 3096–3103.

Arai Y., Marcus M. K., Tamura N., Davis J. A. and Zachara J. M. (2007) Spectroscopic evidence for uranium bearing precipitates in vadose zone sediments at the Hanford 300-area site. *Environ. Sci. Technol.* **41**, 4633–4639.

Bak W. a. (1992) Gram-negative mesophilic sulfate-reducing bacteria. In *The Prokaryotes* (eds. A. Balows, H. G. Trüper, M. Dworkin, W. Harder and K.-H. Schleifer), 2nd ed. Springer, New York, pp. 3352–3378.

Bargar J. R., Reitmeyer R., Lenhart J. J. and Davis J. A. (2000) Characterization of U(VI)-carbonato ternary complexes on hematite: EXAFS and electrophoretic mobility measurements. *Geochim. Cosmochim. Acta* **64**, 2737–2749.

Barnett M. O., Jardine P. M. and Brooks S. C. (2002) U(VI) adsorption to heterogeneous subsurface media: application of a surface complexation model. *Environ. Sci. Technol.* **36**, 937–942.

Barnett M. O., Jardine P. M., Brooks S. C. and Selim H. M. (2000) Adsorption and transport of uranium(VI) in subsurface media. *Soil Sci. Soc. Am. J.* **64**, 908–917.

Beazley M. J., Martinez R. J., Sobecky P. A., Webb S. M. and Taillefert M. (2007) Uranium biomineralization as a result of bacterial phosphatase activity: insights from bacterial isolates from a contaminated subsurface. *Environ. Sci. Technol.* **41**, 5701–5707.

Beazley M. J., Martinez R. J., Sobecky P. A., Webb S. M. and Taillefert M. (2009) Nonreductive biomineralization of uranium(VI) phosphate via microbial phosphatase activity in anaerobic conditions. *Geomicrobiol. J.* **26**, 431–441.

Beazley M. J., Martinez R. J., Webb S. M., Sobecky P. A. and Taillefert M. (2011) The effect of pH and natural microbial phosphatase activity on the speciation of uranium in subsurface soils. *Geochim. Cosmochim. Acta* **75**, 5648–5663.

Becerra C. A., Lopez-Luna E. L., Ergas S. J. and Nuesslein K. (2009) Microcosm-based study of the attenuation of an acid mine drainage-impacted site through biological sulfate and iron reduction. *Geomicrobiol. J.* **26**, 9–20.

Behrends T. and Van Cappellen P. (2005) Competition between enzymatic and abiotic reduction of uranium(VI) under iron reducing conditions. *Chem. Geol.* **220**, 315–327.

Beller H. R. (2005) Anaerobic, nitrate-dependent oxidation of U(IV) oxide minerals by the chemolithoautotrophic bacterium Thiobacillus denitrificans. *Appl. Environ. Microbiol.* **71**, 2170–2174.

Bernier-Latmani R., Veeramani H., Vecchia E. D., Junier P., Lezama-Pacheco J. S., Suvorova E. I., Sharp J. O., Wigginton N. S. and Bargar J. R. (2010) Non-uraninite products of microbial U(VI) reduction. *Environ. Sci. Technol.* **44**, 9456–9462.

Beyenal H., Sani R. K., Peyton B. M., Dohnalkova A. C., Amonette J. E. and Lewandowski Z. (2004) Uranium immobilization by sulfate-reducing biofilms. *Environ. Sci. Technol.* **38**, 2067–2074.

Blakeney M. D., Moulaei T. and DiChristina T. J. (2000) Fe(III) reduction activity and cytochrome content of *Shewanella putrefaciens* grown on ten compounds as sole terminal electron acceptor. *Microbiol. Res.* **155**, 87–94.

Bollag J. M. and Henninger N. M. (1978) Effects of nitrite toxicity on soil bacteria under aerobic and anaerobic conditions. *Soil Biol. Biochem.* **10**, 377–381.

Brooks S. C. (2001) *Waste Characteristics of the Former S-3 Ponds and Outline of Uranium Chemistry Relevant to NABIR Field Research Center Studies*. NABIR FRC.

Brooks S. C., Fredrickson J. K., Carroll S. L., Kennedy D. W., Zachara J. M., Plymale A. E., Kelly S. D., Kemner K. M. and Fendorf S. (2003) Inhibition of bacterial U(VI) reduction by calcium. *Environ. Sci. Technol.* **37**, 1850–1858.

Cardenas E., Wu W.-M., Leigh M. B., Carley J., Carroll S., Gentry T., Luo J., Watson D., Gu B., Ginder-Vogel M., Kitanidis P. K., Jardine P. M., Zhou J., Criddle C. S., Marsh T. L. and Tiedje J. M. (2010) Significant association between sulfate-reducing bacteria and uranium-reducing microbial communities as revealed by a combined massively parallel sequencing-indicator species approach. *Appl. Environ. Microbiol.* **76**, 6778–6786.

Catalano J. G., McKinley J. P., Zachara J. M., Heald S. M., Smith S. C. and Brown G. E. (2006) Changes in uranium speciation through a depth sequence of contaminated Hanford sediments. *Environ. Sci. Technol.* **40**, 2517–2524.

Chakraborty S., Favre F., Banerjee D., Scheinost A. C., Mullet M., Ehrhardt J.-J., Brendle J., Vidal L. and Charlet L. (2010) U(VI) sorption and reduction by Fe(II) sorbed on montmorillonite. *Environ. Sci. Technol.* **44**, 3779–3785.

Cheng T., Barnett M. O., Roden E. E. and Zhuang J. L. (2004) Effects of phosphate on uranium(VI) adsorption to goethite-coated sand. *Environ. Sci. Technol.* **38**, 6059–6065.

Davis J. A. and Kent D. B. (1990) Surface complexation modeling in aqueous geochemistry. *Rev. Mineral.* **23**, 177–260.

Dawson G. W. and Gilman J. (2001) Land reclamation technology – expanding the geotechnical engineering envelope. *Proc. Inst. Civil Eng. – Geotech. Eng.* **149**, 49–61.

De Pablo J., Casas I., Gimenez J., Molera M., Rovira M., Duro L. and Bruno J. (1999) The oxidative dissolution mechanism of uranium dioxide. I. The effect of temperature in hydrogen carbonate medium. *Geochim. Cosmochim. Acta* **63**, 3097–3103.

Dichristina T. J. (1992) Effects of nitrate and nitrite on dissimilatory iron reduction by shewanella-putrefaciens-200. *J. Bacteriol.* **174**, 1891–1896.

DOE (1997) *Linking Legacies – Connecting the Cold War Nuclear Weapons Production Processes to Their Environmental Consequences Office of Environmental Management*. The U.S. Department of Energy Washington, DC.

Dong W. M. and Brooks S. C. (2006) Determination of the formation constants of ternary complexes of uranyl and carbonate with alkaline earth metals (Mg^{2+}, Ca^{2+}, Sr^{2+}, and Ba^{2+}) using anion exchange method. *Environ. Sci. Technol.* **40**, 4689–4695.

Edwards L., Kusel K., Drake H. and Kostka J. E. (2007) Electron flow in acidic subsurface sediments co-contaminated with nitrate and uranium. *Geochim. Cosmochim. Acta* **71**, 643–654.

Finch R. and Murakami T. (1999) Systematics and paragenesis of uranium minerals. *Rev. Mineral. Geochem.* **38**, 91–179.

Finneran K. T., Anderson R. T., Nevin K. P. and Lovley D. R. (2002a) Potential for Bioremediation of uranium-contaminated aquifers with microbial U(VI) reduction. *Soil Sediment Contam.* **11**, 339–357.

Finneran K. T., Housewright M. E. and Lovley D. R. (2002b) Multiple influences of nitrate on uranium solubility during bioremediation of uranium-contaminated subsurface sediments. *Environ. Microbiol.* **4**, 510–516.

Fletcher K. E., Boyanov M. I., Thomas S. H., Wu Q. Z., Kemner K. M. and Loffler F. E. (2010) U(VI) reduction to mononuclear U(IV) by *Desulfitobacterium* species. *Environ. Sci. Technol.* **44**, 4705–4709.

Fox P. M., Davis J. A. and Zachara J. M. (2006) The effect of calcium on aqueous uranium(VI) speciation and adsorption to ferrihydrite and quartz. *Geochim. Cosmochim. Acta* **70**, 1379–1387.

Fredrickson J. K., Zachara J. M., Kennedy D. W., Duff M. C., Gorby Y. A., Li S. M. W. and Krupka K. M. (2000) Reduction of U(VI) in goethite (alpha-FeOOH) suspensions by a dissimilatory metal-reducing bacterium. *Geochim. Cosmochim. Acta* **64**, 3085–3098.

Fredrickson J. K., Zachara J. M., Kennedy D. W., Liu C. X., Duff M. C., Hunter D. B. and Dohnalkova A. (2002) Influence of Mn oxides on the reduction of uranium(VI) by the metal-reducing bacterium *Shewanella putrefaciens*. *Geochim. Cosmochim. Acta* **66**, 3247–3262.

Ganesh R., Robinson K. G., Chu L. L., Kucsmas D. and Reed G. D. (1999) Reductive precipitation of uranium by *Desulfovibrio desulfuricans*: evaluation of cocontaminant effects and selective removal. *Water Res.* **33**, 3447–3458.

Gihring T. M., Zhang G., Brandt C. C., Brooks S. C., Campbell J. H., Carroll S., Criddle C. S., Green S. J., Jardine P., Kostka J. E., Lowe K., Mehlhorn T. L., Overholt W., Watson D. B., Yang Z., Wu W.-M. and Schadt C. W. (2011) A limited microbial consortium is responsible for extended bioreduction of uranium in a contaminated aquifer. *Appl. Environ. Microbiol.* **77**, 5955–5965.

Gleyzes C., Tellier S. and Astruc M. (2002) Fractionation studies of trace elements in contaminated soils and sediments: a review of sequential extraction procedures. *TRAC, Trends Anal. Chem.* **21**, 451–467.

Grasshoff K. (1983) Determination of nitrite. In *Methods of Seawater Analysis* (eds. K. Grasshoff, M. Ehrhardt, K. Kremling and T. Almgren), 2nd, rev. and extended ed. Verlag Chemie GmbH, Weinheim.

Green S. J., Prakash O., Gihring T. M., Akob D. M., Jasrotia P., Jardine P. M., Watson D. B., Brown S. D., Palumbo A. V. and Kostka J. E. (2010) Denitrifying bacteria isolated from terrestrial subsurface sediments exposed to mixed-waste contamination. *Appl. Environ. Microbiol.* **76**, 3244–3254.

Green S. J., Prakash O., Jasrotia P., Overholt W. A., Cardenas E., Hubbard D., Tiedje J. M., Watson D. B., Schadt C. W., Brooks S. C. and Kostka J. E. (2012) Denitrifying bacteria from the genus rhodanobacter dominate bacterial communities in the highly contaminated subsurface of a nuclear legacy waste site. *Appl. Environ. Microbiol.* **78**, 1039–1047.

Gu B. H., Wu W. M., Ginder-Vogel M. A., Yan H., Fields M. W., Zhou J., Fendorf S., Criddle C. S. and Jardine P. M. (2005) Bioreduction of uranium in a contaminated soil column. *Environ. Sci. Technol.* **39**, 4841–4847.

Guillaumont R., Fanghänel T., Fuger J., Grenthe I., Neck V., Palmer D. A. and Rand M. H. (2003) *Chemical Thermodynamics 5. Update on the Checmical Thermodynamics of Uranium, Neptunium, Plutonium, Americium and Technetium*. Elsevier, Amsterdam.

Han R. P., Zou W. H., Wang Y. and Zhu L. (2007) Removal of uranium(VI) from aqueous solutions by manganese oxide coated zeolite: discussion of adsorption isotherms and pH effect. *J. Environ. Radioact.* **93**, 127–143.

Herbert R. A. (1999) Nitrogen cycling in coastal marine ecosystems. *FEMS Microbiol. Rev.* **23**, 563–590.

Ho C. H. and Miller N. H. (1986) Formation of uranium oxide sols in bicarbonate solutions. *J. Colloid Interface Sci.* **113**, 232–240.

Hsi C. K. D. and Langmuir D. (1985) Adsorption of uranyl onto ferric oxyhydroxides – application of the surface complexation site-binding model. *Geochim. Cosmochim. Acta* **49**, 1931–1941.

Hudson E. A., Allen P. G., Terminello L. J., Denecke M. A. and Reich T. (1996) Polarized X-ray-absorption spectroscopy of the uranyl ion: comparison of experiment and theory. *Phys. Rev. B* **54**, 156.

Hyun S. P., Davis J. A., Sun K. and Hayes K. F. (2012) Uranium(VI) reduction by iron(II) monosulfide mackinawite. *Environ. Sci. Technol.* **46**, 3369–3376.

Istok J. D., Senko J. M., Krumholz L. R., Watson D., Bogle M. A., Peacock A., Chang Y. J. and White D. C. (2004) In situ bioreduction of technetium and uranium in a nitrate-contaminated aquifer. *Environ. Sci. Technol.* **38**, 468–475.

Jardine P. M., Watson D. B, Blake D. A., Beard L. P., Brooks S. C., Carley J. M., Criddle C. S., Doll W. E., Fields M. W., Fendorf S. E., Geesey G. G., Ginder-Vogel M., Hubbard S. S., Istok J. D., Kelly S., Kemner K. M., Peacock A. D., Spalding B. P., White D. C., Wolfe A., Wu W. and Zhou J. (2006) Techniques for assessing the performance of in situ bioreduction and immobilization of metals and radionuclides in contaminated subsurface environments. Technical Report, NABIR FRC.

Jeon B. H., Dempsey B. A., Burgos W. D., Barnett M. O. and Roden E. E. (2005) Chemical reduction of U(VI) by Fe(II) at the solid-water interface using natural and synthetic Fe(III) oxides. *Environ. Sci. Technol.* **39**, 5642–5649.

Jeon B. H., Kelly S. D., Kemner K. M., Barnett M. O., Burgos W. D., Dempsey B. A. and Roden E. E. (2004) Microbial reduction of U(VI) at the solid-water interface. *Environ. Sci. Technol.* **38**, 5649–5655.

Jerden J. L. and Sinha A. K. (2003) Phosphate based immobilization of uranium in an oxidizing bedrock aquifer. *Appl. Geochem.* **18**, 823–843.

Katsoyiannis I. A. (2007) Carbonate effects and pH-dependence of uranium sorption onto bacteriogenic iron oxides: kinetic and equilibrium studies. *J. Hazard. Mater.* **139**, 31–37.

Kelly S. D., Kemner K. M., O'Loughlin E. J., Boyanov M. I., Watson D. B., Jardine P. M. and Phillips D. H. (2005) U L3-Edge EXAFS Measurements of Sediment Samples from Oak Ridge National Laboratory, Tennessee, U.S.A. Technical Report.

Kelly S. D., Wu W.-M., Yang F., Criddle C. S., Marsh T. L., O'Loughlin E. J., Ravel B., Watson D., Jardine P. M. and Kemner K. M. (2009) Uranium transformations in static microcosms. *Environ. Sci. Technol.* **44**, 236–242.

Kim O.-H., Kim Y.-O., Shim J.-H., Jung Y.-S., Jung W.-J., Choi W.-C., Lee H., Lee S.-J., Kim K.-K., Auh J.-H., Kim H., Kim J.-W., Oh T.-K. and Oh B.-C. (2010) Beta-propeller phytase hydrolyzes insoluble Ca(2+)-phytate salts and completely abrogates the ability of phytate to chelate metal ions. *Biochemistry* **49**, 10216–10227.

Kostka J. E. and Green S. J. (2011) Microorganisms and processes linked to uranium reduction and immobilization. In *Microbial Metal and Metalloid Metabolism: Advances and Applications* (eds. J. F. Stolz and R. S. Oremland). ASM Press, Washington, DC, pp. 117–138.

Kosztolanyi K., Nguyen T. C., Lhote F. and Vernet M. (1996) Reduction of uranyl complexes and precipitation of uranium

oxides by means of hydrogen sulphide gas. *Magy. Kem. Foly.* **102**, 180–187.

Langmuir D. (1997) *Aqueous Environmental Geochemistry*. Prentice Hall, Upper Saddle River, New Jersey.

Ler A. and Stanforth R. (2003) Evidence for surface precipitation of phosphate on goethite. *Environ. Sci. Technol.* **37**, 2694–2700.

Li L. and Stanforth R. (2000) Distinguishing adsorption and surface precipitation of phosphate on goethite (alpha-FeOOH). *J. Colloid Interface Sci.* **230**, 12–21.

Liger E., Charlet L. and Van Cappellen P. (1999) Surface catalysis of uranium(VI) reduction by iron(II). *Geochim. Cosmochim. Acta* **63**, 2939–2955.

Liu C. X., Zachara J. M., Fredrickson J. K., Kennedy D. W. and Dohnalkova A. (2002) Modeling the inhibition of the bacterial reduction of U(VI) by beta-MnO_2(S)(g). *Environ. Sci. Technol.* **36**, 1452–1459.

Liu C. X., Zachara J. M., Qafoku O., McKinley J. P., Heald S. M. and Wang Z. M. (2004) Dissolution of uranyl microprecipitates in subsurface sediments at Hanford site, USA. *Geochim. Cosmochim. Acta* **68**, 4519–4537.

Lovley D. R. (1993) Dissimilatory metal reduction. *Annu. Rev. Microbiol.* **47**, 263–290.

Lovley D. R. and Phillips E. J. P. (1992) Reduction of uranium by desulfovibrio-desulfuricans. *Appl. Environ. Microbiol.* **58**, 850–856.

Lovley D. R., Phillips E. J. P., Gorby Y. A. and Landa E. R. (1991) Microbial reduction of uranium. *Nature* **350**, 413–416.

Luo J., Weber F. A., Cirpka O. A., Wu W. M., Nyman J. L., Carley J., Jardine P. M., Criddle C. S. and Kitanidis P. K. (2007) Modeling in-situ uranium(VI) bioreduction by sulfate-reducing bacteria. *J. Contam. Hydrol.* **92**, 129–148.

Macaskie L. E., Empson R. M., Cheetham A. K., Grey C. P. and Skarnulis A. J. (1992) Uranium bioaccumulation by a *Citrobacter* sp. as a result of enzymatically mediated growth of polycrystalline HUO_2PO_4. *Science* **257**, 782–784.

Macaskie L. E., Hewitt C. J., Shearer J. A. and Kent C. A. (1995) Biomass production for the removal of heavy-metals from aqueous-solutions at low pH using growth-decoupled cells of a *Citrobacter* sp. *Int. Biodeterior. Biodegrad.* **35**, 73–92.

Mackay D. M. and Cherry J. A. (1989) Groundwater contamination: pump-and-treat remediation part 2. *Environ. Sci. Technol.* **23**, 630–636.

Madden A. S., Palumbo A. V., Ravel B., Vishnivetskaya T. A., Phelps T. J., Schadt C. W. and Brandt C. C. (2009) Donor-dependent extent of uranium reduction for bioremediation of contaminated sediment microcosms. *J. Environ. Qual.* **38**, 53–60.

Madden A. S., Smith A. C., Balkwill D. L., Fagan L. A. and Phelps T. J. (2007) Microbial uranium immobilization independent of nitrate reduction. *Environ. Microbiol.* **9**, 2321–2330.

Marsili E., Beyenal H., Di Palma L., Merli C., Dohnalkova A., Amonette J. E. and Lewandowski Z. (2007) Uranium immobilization by sulfate-reducing biofilms grown on hematite, dolomite, and calcite. *Environ. Sci. Technol.* **41**, 8349–8354.

Martinez R. J., Beazley M. J., Taillefert M., Arakaki A. K., Skolnick J. and Sobecky P. A. (2007) Aerobic uranium (VI) bioprecipitation by metal-resistant bacteria isolated from radionuclide- and metal-contaminated subsurface soils. *Environ. Microbiol.* **9**, 3122–3133.

Martinez R. J., Wang Y. L., Raimondo M. A., Coombs J. M., Barkay T. and Sobecky P. A. (2006) Horizontal gene transfer of P-IB-type ATPases among bacteria isolated from radionuclide- and metal-contaminated subsurface soils. *Appl. Environ. Microbiol.* **72**, 3111–3118.

Meijer E. M., Vanderzwaan J. W., Wever R. and Stouthamer A. H. (1979) Anaerobic respiration and energy-conservation in paracoccus-denitrificans – functioning of iron–sulfur centers and the uncoupling effect of nitrite. *Eur. J. Biochem.* **96**, 69–76.

Meleshyn A., Azeroual M., Reeck T., Houben G., Riebe B. and Bunnenberg C. (2009) Influence of (calcium–)uranyl–carbonate complexation on U(VI) sorption on Ca- and Na-bentonites. *Environ. Sci. Technol.* **43**, 4896–4901.

Mohagheghi A., Updegraff D. M. and Goldhaber M. B. (1985) The role of sulfate-reducing bacteria in the deposition of sedimentary uranium ores. *Geomicrobiol. J.* **4**, 153–173.

Mohanty S. R., Kollah B., Hedrick D. B., Peacock A. D., Kukkadapu R. K. and Roden E. E. (2008) Biogeochemical processes in ethanol stimulated uranium-contaminated subsurface sediments. *Environ. Sci. Technol.* **42**, 4384–4390.

Montgomery D. M., Dean A. C. R., Wiffen P. and Macaskie L. E. (1995) Phosphatase production and activity in citrobacter-freundii and a naturally-occurring, heavy-metal-accumulating *Citrobacter* sp. *Microbiology* **141**, 2433–2441.

Moon H. S., Komlos J. and Jaffe P. R. (2007) Uranium reoxidation in previously bioreduced sediment by dissolved oxygen and nitrate. *Environ. Sci. Technol.* **41**, 4587–4592.

Murphy J. and Riley J. P. (1962) A modified single solution method for determination of phosphate in natural waters. *Anal. Chim. Acta* **26**.

Murphy W. M. and Shock E. L. (1999) Environmental aqueous geochemistry of actinides. In *Uranium: Mineralogy, Geochemistry and the Environment* (eds. P. C. A. Burns and R. Finch). Mineralogical Society of America, Washington, DC.

NABIR (2003) Bioremediation of Metals and Radionuclides, DOE.

North N. N., Dollhopf S. L., Petrie L., Istok J. D., Balkwill D. L. and Kostka J. E. (2004) Change in bacterial community structure during in situ biostimulation of subsurface sediment cocontaminated with uranium and nitrate. *Appl. Environ. Microbiol.* **70**, 4911–4920.

Nriagu J. O. (1972) Stability of vivianite and ion-pair formation in system $Fe_3(PO_4)_2$–H_3PO_4–H_2O. *Geochim. Cosmochim. Acta* **36**, 459–470.

Nyman J. L., Marsh T. L., Ginder-Vogel M. A., Gentile M., Fendorf S. and Criddle C. (2006) Heterogeneous response to biostimulation for U(VI) reduction in replicated sediment microcosms. *Biodegradation* **17**, 303–316.

Ohnuki I., Kozai N., Samadfam M., Yasuda R., Yamamoto S., Narumi K., Naramoto H. and Murakami T. (2004) The formation of autunite (Ca(UO2)(2)(PO4)(2)·*n*H(2)O)within the leached layer of dissolving apatite: incorporation mechanism of uranium by apatite. *Chem. Geol.* **211**, 1–14.

Payne T. E., Davis J. A. and Waite T. D. (1996) Uranium adsorption on ferrihydrite – effects of phosphate and humic acid. *Radiochim. Acta* **74**, 239–243.

Petrie L., North N. N., Dollhopf S. L., Balkwill D. L. and Kostka J. E. (2003) Enumeration and characterization of iron(III)-reducing microbial communities from acidic subsurface sediments contaminated with uranium(VI). *Appl. Environ. Microbiol.* **69**, 7467–7479.

Qatibi A. I., Niviere V. and Garcia J. L. (1991) *Desulfovibrio-alcoholovorans* sp. nov., a sulfate-reducing bacterium able to grow on glycerol, 1,2-propanediol and 1,3-propanediol. *Arch. Microbiol.* **155**, 143–148.

Rake J. B. and Eagon R. G. (1980) Inhibition, but not uncoupling, of respiratory energy coupling of 3 bacterial species by nitrite. *J. Bacteriol.* **144**, 975–982.

Regenspurg S., Schild D., Schafer T., Huber F. and Malmstrom M. E. (2009) Removal of uranium(VI) from the aqueous phase by iron(II) minerals in presence of bicarbonate. *Appl. Geochem.* **24**, 1617–1625.

Roh Y., Lee S. R., Choi S. K., Elless M. P. and Lee S. Y. (2000) Physicochemical and mineralogical characterization of uranium-contaminated soils. *Soil Sediment Contam.* **9**, 463–486.

Rossolini G. M., Schippa S., Riccio M. L., Berlutti F., Macaskie L. E. and Thaller M. C. (1998) Bacterial nonspecific acid phosphohydrolases: physiology, evolution and use as tools in microbial biotechnology. *Cell. Mol. Life Sci.* **54**, 833–850.

Sanford R. A., Wu Q., Sung Y., Thomas S. H., Amos B. K., Prince E. K. and Loffler F. E. (2007) Hexavalent uranium supports growth of *Anaeromyxobacter dehalogenans* and *Geobacter* spp. with lower than predicted biomass yields. *Environ. Microbiol.* **9**, 2885–2893.

Schecher W. D. and McAvoy D. C. (2001) MINEQL+: A Chemical Equilibrium Modeling System, Version 4.5 for Windows, User's Manual. Research Software, Hallowell, Maine.

Senko J. M., Istok J. D., Suflita J. M. and Krumholz L. R. (2002) In-situ evidence for uranium immobilization and remobilization. *Environ. Sci. Technol.* **36**, 1491–1496.

Senko J. M., Mohamed Y., Dewers T. A. and Krumholz L. R. (2005a) Role for Fe(III) minerals in nitrate-dependent microbial U(IV) oxidation. *Environ. Sci. Technol.* **39**, 2529–2536.

Senko J. M., Suflita J. M. and Krumholz L. R. (2005b) Geochemical controls on microbial nitrate-dependent U(IV) oxidation. *Geomicrobiol. J.* **22**, 371–378.

Sharp J. O., Lezama-Pacheco J. S., Schofield E. J., Junier P., Ulrich K.-U., Chinni S., Veeramani H., Margot-Roquier C., Webb S. M., Tebo B. M., Giammar D. E., Bargar J. R. and Bernier-Latmani R. (2011) Uranium speciation and stability after reductive immobilization in aquifer sediments. *Geochim. Cosmochim. Acta* **75**, 6497–6510.

Shelobolina E. S., Konishi H., Xu H. F. and Roden E. E. (2009) U(VI) sequestration in hydroxyapatite produced by microbial glycerol 3-phosphate metabolism. *Appl. Environ. Microbiol.* **75**, 5773–5778.

Shelobolina E. S., O'Neill K., Finneran K. T., Hayes L. A. and Lovley D. R. (2003) Potential for in situ bioremediation of a low-pH, high-nitrate uranium-contaminated groundwater. *Soil Sediment Contam.* **12**, 865–884.

Sijbesma W. F. H., Almeida J. S., Reis M. A. M. and Santos H. (1996) Uncoupling effect of nitrite during denitrification by Pseudomonas fluorescens: an in vivo P-31-NMR study. *Biotechnol. Bioeng.* **52**, 176–182.

Singer P. C. and Stumm W. (1970) Solubility of ferrous iron in carbonate-bearing waters. *J. Am. Water Works Assoc.* **62**, 198–202.

Sowder A. G., Clark S. B. and Fjeld R. A. (2001) The impact of mineralogy in the U(VI)–Ca–PO_4 system on the environmental availability of uranium. *J. Radioanal. Nucl. Chem.* **248**, 517–524.

Spain A. M. and Krumholz L. R. (2011) Nitrate-reducing bacteria at the nitrate and radionuclide contaminated Oak Ridge integrated field research challenge site: a review. *Geomicrobiol. J.* **28**, 418–429.

Stewart B. D., Mayes M. A. and Fendorf S. (2010) Impact of uranyl–calcium–carbonato complexes on uranium(VI) adsorption to synthetic and natural sediments. *Environ. Sci. Technol.* **44**, 928–934.

Stookey L. L. (1970) Ferrozine – a new spectrophotometric reagent for iron. *Anal. Chem.* **42**, 779–781.

Stubbs J. E., Elbert D. C., Veblen D. R. and Zhu C. (2006) Electron microbeam investigation of uranium-contaminated soils from Oak Ridge, TN, USA. *Environ. Sci. Technol.* **40**, 2108–2113.

Stumm W. and Morgan J. J. (1996) *Aquatic Chemistry: Chemical Equilibria and Rates in Natural Waters*, 3rd ed. Wiley, New York.

Tessier A., Campbell P. G. C. and Bisson M. (1979) Sequential extraction procedure for the speciation of particulate trace-metals. *Anal. Chem.* **51**, 844–851.

Ulrich K. U., Ilton E. S., Veeramani H., Sharp J. O., Bernier-Latmani R., Schofield E. J., Bargar J. R. and Giammar D. E. (2009) Comparative dissolution kinetics of biogenic and chemogenic uraninite under oxidizing conditions in the presence of carbonate. *Geochim. Cosmochim. Acta* **73**, 6065–6083.

Van Haverbeke L., Vochten R. and Van Springel K. (1996) Solubility and spectrochemical characteristics of synthetic chernikovite and meta-ankoleite. *Mineral. Mag.* **60**, 759–766.

Wade R. and DiChristina T. J. (2000) Isolation of U(VI) reduction-deficient mutants of *Shewanella putrefaciens*. *FEMS Microbiol. Lett.* **184**, 143–148.

Waite T. D., Davis J. A., Payne T. E., Waychunas G. A. and Xu N. (1994) Uranium(VI) adsorption to ferrihydrite-application of a surface complexation model. *Geochim. Cosmochim. Acta* **58**, 5465–5478.

Wan J. M., Tokunaga T. K., Brodie E., Wang Z. M., Zheng Z. P., Herman D., Hazen T. C., Firestone M. K. and Sutton S. R. (2005) Reoxidation of bioreduced uranium under reducing conditions. *Environ. Sci. Technol.* **39**, 6162–6169.

Webb S. M. (2005) SIXpack: a graphical user interface for XAS analysis using IFEFFIT. *Phys. Scr.* **T115**, 1011–1014.

Webb S. M., Fuller C. C., Tebo B. M. and Bargar J. R. (2006) Determination of uranyl incorporation into biogenic manganese oxides using X-ray absorption spectroscopy and scattering. *Environ. Sci. Technol.* **40**, 771–777.

Webb S. M., Tebo B. M. and Bargat J. R. (2005) Structural characterization of biogenic Mn oxides produced in seawater by the marine bacillus sp strain SG-1. *Am. Mineral.* **90**, 1342–1357.

Wellman D. M., Gunderson K. M., Icenhower J. P. and Forrester S. W. (2007) Dissolution kinetics of synthetic and natural meta-autunite minerals, X-3-$n((n)+)(UO_2)(PO_4)(2)$ center dot xH(2)O, under acidic conditions. *Geochem. Geophys. Geosyst.* **8**.

Wellman D. M., Icenhower J. P. and Owen A. T. (2006) Comparative analysis of soluble phosphate amendments for the remediation of heavy metal contaminants: effect on sediment hydraulic conductivity. *Environ. Chem.* **3**, 219–224.

Wersin P., Hochella M. F., Persson P., Redden G., Leckie J. O. and Harris D. W. (1994) Interaction between aqueous uranium(VI) and sulfide minerals – spectroscopic evidence for sorption and reduction. *Geochim. Cosmochim. Acta* **58**, 2829–2843.

Wielinga B., Bostick B., Hansel C. M., Rosenzweig R. F. and Fendorf S. (2000) Inhibition of bacterially promoted uranium reduction: ferric (hydr)oxides as competitive electron acceptors. *Environ. Sci. Technol.* **34**, 2190–2195.

Wu W. M., Carley J., Fienen M., Mehlhorn T., Lowe K., Nyman J., Luo J., Gentile M. E., Rajan R., Wagner D., Hickey R. F., Gu B. H., Watson D., Cirpka O. A., Kitanidis P. K., Jardine P. M. and Criddle C. S. (2006a) Pilot-scale in situ bioremediation of uranium in a highly contaminated aquifer. 1. Conditioning of a treatment zone. *Environ. Sci. Technol.* **40**, 3978–3985.

Wu W. M., Carley J., Gentry T., Ginder-Vogel M. A., Fienen M., Mehlhorn T., Yan H., Caroll S., Pace M. N., Nyman J., Luo J., Gentile M. E., Fields M. W., Hickey R. F., Gu B. H., Watson D., Cirpka O. A., Zhou J. Z., Fendorf S., Kitanidis P. K., Jardine P. M. and Criddle C. S. (2006b) Pilot-scale in situ bioremedation of uranium in a highly contaminated aquifer. 2. Reduction of U(VI) and geochemical control of U(VI) bioavailability. *Environ. Sci. Technol.* **40**, 3986–3995.

Wu W. M., Carley J., Green S. J., Luo J. A., Kelly S. D., Van Nostrand J., Lowe K., Mehlhorn T., Carroll S., Boonchayanant B., Lofller F. E., Watson D., Kemner K. M., Zhou J. Z.,

Kitanidis, Kostka J. E., Jardine P. M. and Criddle C. S. () Effects of nitrate on the stability of uranium in a bioreduced region of the subsurface. *Environ. Sci. Technol.* **44**, 5104–5111.

Zabinsky S. I., Rehr J. J., Ankudinov A., Albers R. C. and Eller M. J. (1995) Multiple-scattering calculations of X-ray absorption spectra. *Phys. Rev. B* **52**, 2995–3009.

Zhang F., Wu W.-M., Parker J. C., Mehlhorn T., Kelly S. D., Kemner K. M., Zhang G., Schadt C., Brooks S. C., Criddle C. S., Watson D. B. and Jardine P. M. (2010) Kinetic analysis and modeling of oleate and ethanol stimulated uranium (VI) bio-reduction in contaminated sediments under sulfate reduction conditions. *J. Hazard. Mater.* **183**, 482–489.

Zheng Z. P., Tokunaga T. K. and Wan J. M. (2003) Influence of calcium carbonate on U(VI) sorption to soils. *Environ. Sci. Technol.* **37**, 5603–5608.

Zheng Z. P., Wan J. M., Song X. Y. and Tokunaga T. K. (2006) Sodium meta-autunite colloids: Synthesis, characterization, and stability. *Colloids Surf. A – Physicochem. Eng. Aspects* **274**, 48–55.

Associate editor: Owen Duckworth